Seismic attribute analysis and CO_2 monitoring within the Mississippian reservoir, Wellington field, Sumner County, Kansas

By

Lauren Haga
B.Sc., University of Kansas, 2016

Submitted to the graduate degree program in Geology and the Graduate Faculty of the University of Kansas in partial fulfillment of the requirements for the degree of Master of Science.

_____

Chair: Dr. George Tsoflias

_____

Dr. Ross Black

_____

Dr. Anthony Walton

Date Defended: 9 May 2019

The thesis committee for Lauren Haga certifies that this is the approved version of the following thesis:

Seismic attribute analysis and CO_2 monitoring within the Mississippian reservoir, Wellington field, Sumner County, Kansas

Chair: Dr. George Tsoflias

Date Approved: 17 May 2019

ABSTRACT

The Mississippian reservoirs are prolific hydrocarbon producers in the mid-continent of the United States but are challenging to image seismically due to their high heterogeneity and thicknesses typically below seismic resolution. In 2016, the Kansas Geological Survey (KGS) conducted a pilot study in the Mississippian chert reservoir at Wellington field, Sumner County, Kansas to determine the feasibility of injecting CO_2 for enhanced oil recovery (EOR) and geologic storage of CO_2 in this geological environment.

This study evaluates the use of seismic methods for imaging the injected CO_2 in the Mississippian reservoir. Time-lapse seismic comparison of an arbitrary line extracted from the pre-injection 3-D seismic survey and a coincident post-injection 2-D line proved ineffective due to differences between a 3-D volume and 2-D profile imaging. Therefore, imaging the CO_2 centered on analysis of the post-injection 2-D seismic line characteristics both near to and far from the injection well, KGS #2-32, where CO_2 saturation varied from 50% to 0% respectively. Fluid substitution modeling was used to evaluate Mississippian reservoir acoustic property changes due to CO_2 saturation changes. CO_2 saturation levels of 10%, 25%, and 50% displayed a decrease (larger absolute value) in normal-incidence acoustic impedance of up to 2.4%, 6.1%, and 13.3% with increasing CO_2 saturation, respectively. Amplitude Variation with Offset (AVO) analysis of the post-injection 2-D seismic line evaluated the amplitude response at seismic gathers near to and far from the injection well. The majority of the CDP's (including CDP 203230 – location of KGS #2-32) exhibit significant scatter but an overall decrease in amplitude magnitude with offset is present indicating a Class I AVO response of the Mississippian reservoir. Noise identified in the gathers was suppressed using f-k filtering; however, intercept-gradient crossplots and gradient curves throughout the seismic line were too

scattered to reliably identify changes in CO_2 saturation. Three factors contributed to the negative result: 1) Class I AVO increasing impedance, high matrix incompressibility of carbonate reservoirs make fluid detection challenging, 2) a relatively small amount of CO_2 (20,000 tons) was injected in the reservoir and 3) poor near surface conditions during data acquisition resulted in noisy seismic data. Although these challenges made it difficult to image the injected CO_2 in the field, fluid substitution modeling suggests a decrease in normal-incidence acoustic impedance with increasing CO_2 saturation, which may yield detectable changes in seismic data under favorable field conditions.

ACKNOWLEDGEMENTS

I would like to thank everyone who has supported me throughout the completion of my Master of Science degree in geophysics from the University of Kansas. My research project was supported through grants from the US Department of Energy (DOE) contract (DE-FE0006821). The project was also supported by the Kansas Geological Survey (KGS) and the Kansas Interdisciplinary Carbonate Consortium (KICC).

First of all, I would like to thank my academic advisor, Dr. George Tsoflias, for his support throughout my research. In addition to our many hours of collaboration and discussion, as well as, teaching me how to complete a research project with minor supervision. I would also like to thank my committee members, Dr. Ross Black and Dr. Anthony Walton, for their interest in my project, valuable insights, and help with reviewing my thesis proposal and thesis. I am also thankful to Eugene Holubnyak at the KGS for providing useful information and data for fluid substitution modeling, Brandon Graham for his previous work completed in fluid substitution modeling using arbitrary values to create guidelines for expectations of post-injection modeling, and Dr. Lynn Watney for supporting this work. The seismic data used in this research project was acquired by Paragon Geophysical Services Inc. and processed by FairfieldNodal. In addition, I am thankful to CGG for providing the University of Kansas with Hampson-Russell Software. This research project is part of a larger project in south-central Kansas funded by Kansas Geological Survey and the DOE. I am extremely grateful for the KGS and everyone involved with this project for providing me with seismic data, useful information, valuable insight, and support.

Finally, I am extremely thankful to my parents, Deborah and Gary Haga, for supporting me through this experience. Also, I am grateful to my sister, Leah Whitmer, for all of her

support, and my grandparents, Richard and Dianne Radman. They have all supported me greatly throughout this entire experience and my whole life.

Table of Contents

LIST OF FIGURES AND TABLES

Figures

Tables

CHAPTER 1: INTRODUCTION

The Mississippian reservoir at Wellington oil field, south-central Kansas was discovered on December 4, 1929 (Figure 1.1.1). In 1937, the Lansing-Kansas City reservoir was discovered in Wellington field. As of November 2018, there are 55 active wells in the field, and it has produced 20.86 million cumulative barrels of oil from the Mississippian Osagean and Lansing-Kansas City reservoirs (Kansas Geological Survey website, 2018). Oil recovery from the Mississippian has been aided by water flooding. In south-central Kansas, the Mississippian is a highly heterogeneous cherty dolomite reservoir with unit thicknesses typically below seismic resolution; therefore, making it challenging to characterize using seismic imaging methods. Development of Wellington field has been guided primarily by subsurface data (Watney et al., 2013).

The Mississippian reservoir exhibits a downward gradational decrease in porosity resulting in an increase in acoustic velocity. Earlier studies by Sirazhiev (2012) and Fadolalkarem (2015) exploited this characteristic velocity trend as well as analysis of 3-D seismic data to predict reservoir thickness and porosity distribution. However, it is not known if seismic imaging can detect changes in reservoir pore fluid at Wellington. A relatively small amount, approximately 20,000 metric tons, of CO_2 was injected into the Mississippian reservoir at Wellington field in a supercritical state from January 9 to June 21, 2016 (Holubnyak et al., 2017). The purpose of this study is to evaluate the utility of surface seismic reflection for imaging the CO_2 that was injected into the Mississippian reservoir.

The CO_2 injection at Wellington field was a pilot study conducted by the Kansas Geological Survey (KGS) to determine enhanced oil recovery (EOR) viability in carbonate reservoirs and to evaluate the utilization of EOR for potential CO_2 storage (Holubnyak et al.,

2017). Therefore, there is interest in evaluating technologies for monitoring the fate of the injected CO_2. Seismic data was acquired pre- and post-CO_2 injection to monitor the CO_2 plume within the Mississippian reservoir. Paragon Geophysical Services Inc. acquired two 2-D seismic lines and one 3-D seismic survey pre-injection in 2010, and one post-injection 2-D seismic line acquired in summer 2016. The post-injection seismic line crosses west to east through the 3-D pre-injection seismic survey and the injection well, KGS #2-32, but does not directly overlie either of the pre-injection 2-D seismic lines (Figure 1.1.2). Therefore, an arbitrary line was extracted from the pre-injection 3-D seismic survey to directly overlay the post-injection seismic line. Initially, all pre-injection seismic data was processed by FairfieldNodal in 2010-2011 and re-processed by the same company in 2016, including the post-injection 2-D line. The data was re-processed with the goal of preserving rock properties and amplitude variation information in the seismic records by applying less severe noise suppression workflows. Re-processing of the seismic data ultimately resulted in noisier data but a more accurate relative amplitude content (KGS Data Release, 2016). The arbitrary line extracted from the 3-D volume was compared to the coincident post-injection 2-D line for time-lapse seismic analysis; however, inherent differences between 3-D and 2-D seismic imaging dominated data quality inhibiting the time-lapse analysis. Next, multiple seismic analysis methods were applied to the 2-D post-injection seismic dataset to possibly identify differences near and far from the injection well where CO_2 is known to be present or absent from the reservoir. Seismic analysis techniques applied include fluid substitution modeling and amplitude variation with offset (AVO) analysis.

Fluid substitution modeling is a common seismic analysis method used to determine how the introduction of a fluid into the reservoir pore space affects seismic velocities through modeling various possible fluid scenarios at the injection site (Smith et al., 2003; Arts et al.,

2004). While it is a common method used, fluid substitution modeling presents multiple challenges in carbonates such as the Mississippian reservoir but works relatively well in clastics. There are two main types of fluid substitution modeling: Gassmann and patchy; both types were evaluated in this study. Although both types were analyzed, patchy saturation is thought to be a better fit for CO_2/H_2O saturated carbonate rocks. This is because Gassmann theory assumes a homogeneous medium. In addition, Graham, Tsoflias, and Watney (2016) investigated the effects of both Gassmann and patchy fluid substitution in the Mississippian reservoir at Wellington field using 0 to 100% CO_2 saturation with a sample interval of 2%. The rest of the space was filled with water in their simulations; oil saturation was not taken into account. They concluded that while both models predict an amplitude decrease with increasing CO_2 saturation, patchy modeling will be more effective for saturations greater than 20% and Gassmann modeling will display higher resolution for 2-10% CO_2 saturation. Therefore, both theory and recent studies by Graham et al. (2016) were taken into account when deciding which fluid substitution model would be most effective for this dataset.

To supplement fluid substitution modeling, I completed amplitude variation with offset (AVO) analysis of the post-injection 2-D seismic line. Similar to fluid substitution modeling, amplitude variation with offset is another common seismic analysis technique utilized to determine pore fluids, e.g. CO_2 saturation, in a reservoir (Brown et al., 2007). Standard AVO attributes, intercept (A) and gradient (B), were crossplotted and analyzed at the Mississippian reservoir in Wellington field. AVO crossplots are utilized to derive hydrocarbon indicators from seismic data. Each crossplot exhibits a background trend which passes through the origin and is typically assumed to have a negative slope. The background trend is extremely useful in identifying hydrocarbons or unusual lithologies since any deviations from the trend are indicative

of both of these (Castagna and Swan, 1997; Castagna et al., 1998). In addition to identifying hydrocarbons, AVO crossplots are commonly used to monitor CO_2 saturation. The A-B crossplots and gradient curves derived from the analysis of the 2-D post-CO_2 injection line showed large scatter and therefore, were not able to successfully identify changes in CO_2 saturation; however, I was able to identify the Mississippian reservoir at the injection site (KGS #2-32) as a Class I AVO anomaly.

Utilizing these seismic analysis methods to monitor a CO_2 injection is a lot more common in clastic reservoirs than carbonate reservoirs. Carbonate reservoirs present multiple challenges that clastics do not, including a relatively incompressible matrix and heterogeneity (Lumley, 2001). Therefore, more case studies analyzing the ability of time-lapse seismic, fluid substitution modeling, and AVO analysis to monitor a CO_2 injection in a clastic setting have been completed in varying field sites throughout the world. Two of the better researched clastic field sites include the Sleipner field in the North Sea and the Ketzin site in Germany (Chadwick et al., 2010; Ivanova et al., 2013). The injection at Sleipner field was one of the first injections into a saline aquifer with the target reservoir being the Utsira sand; while the Ketzin site primarily consisted of lithologically heterogeneous sandstones. Time-lapse seismic analysis was completed at both fields, and they discovered that it is an extremely useful analysis method when the proper data is acquired. Both studies injected a larger amount of CO_2 in the subsurface than the pilot-study completed by the KGS, which makes it easier to monitor and image the CO_2 using these methods (Arts et al., 2004; Ivanova et al., 2013). In particular, the Ketzin site injected approximately 64,000 tons, more than three times the amount injected in our study, and they were able to successfully monitor CO_2 storage using AVO analysis and fluid substitution (Ivanova et al., 2013). As previously stated, it is a lot more common to monitor CO_2 in a clastic

reservoir using these seismic analysis methods due to the challenges present when working in a carbonate reservoir, such as heterogeneity and high matrix incompressibility. In addition to the common challenges present in most case studies when monitoring CO_2 in a carbonate reservoir, our study is faced with additional challenges including the relatively small amount of CO_2 injected into the reservoir and working with a thin reservoir (the Mississippian reservoir in our case study) which is below seismic resolution.

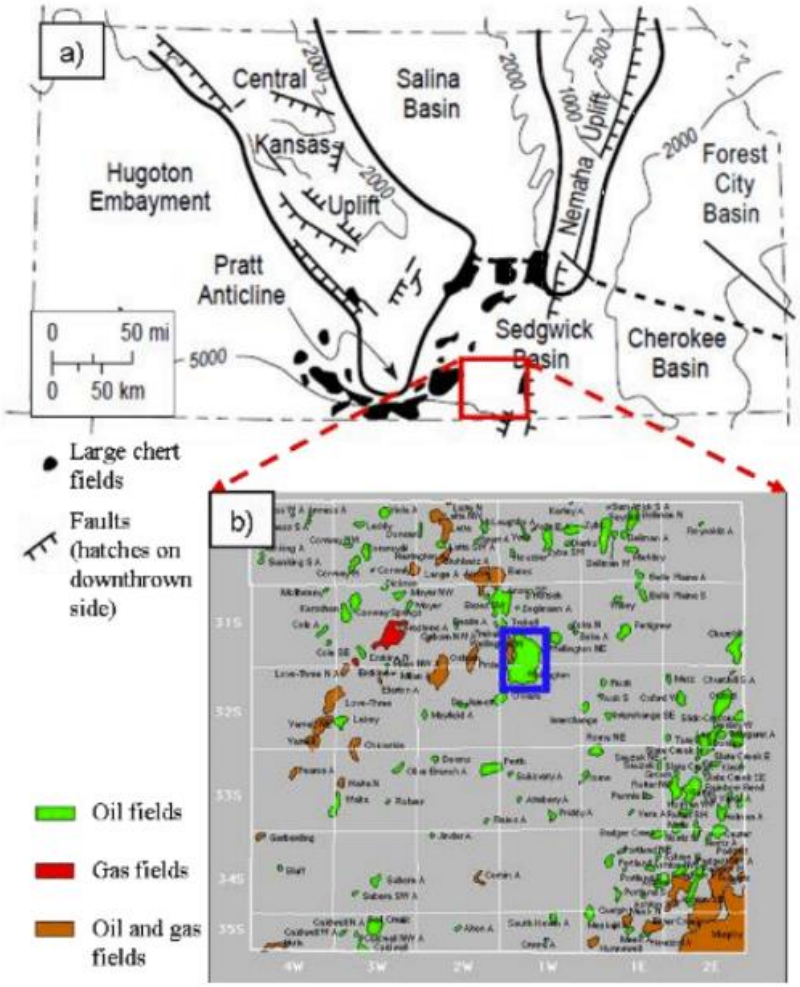

Figure 1.1.1. a) Map of the State of Kansas illustrating major structural features, hydrocarbon producing areas and the location of Sumner County, Kansas outlined in the red box. b) Map of all oil and gas fields in Sumner County displayed with Wellington field, the study area, outlined by the blue box (Sirazhiev, 2012).

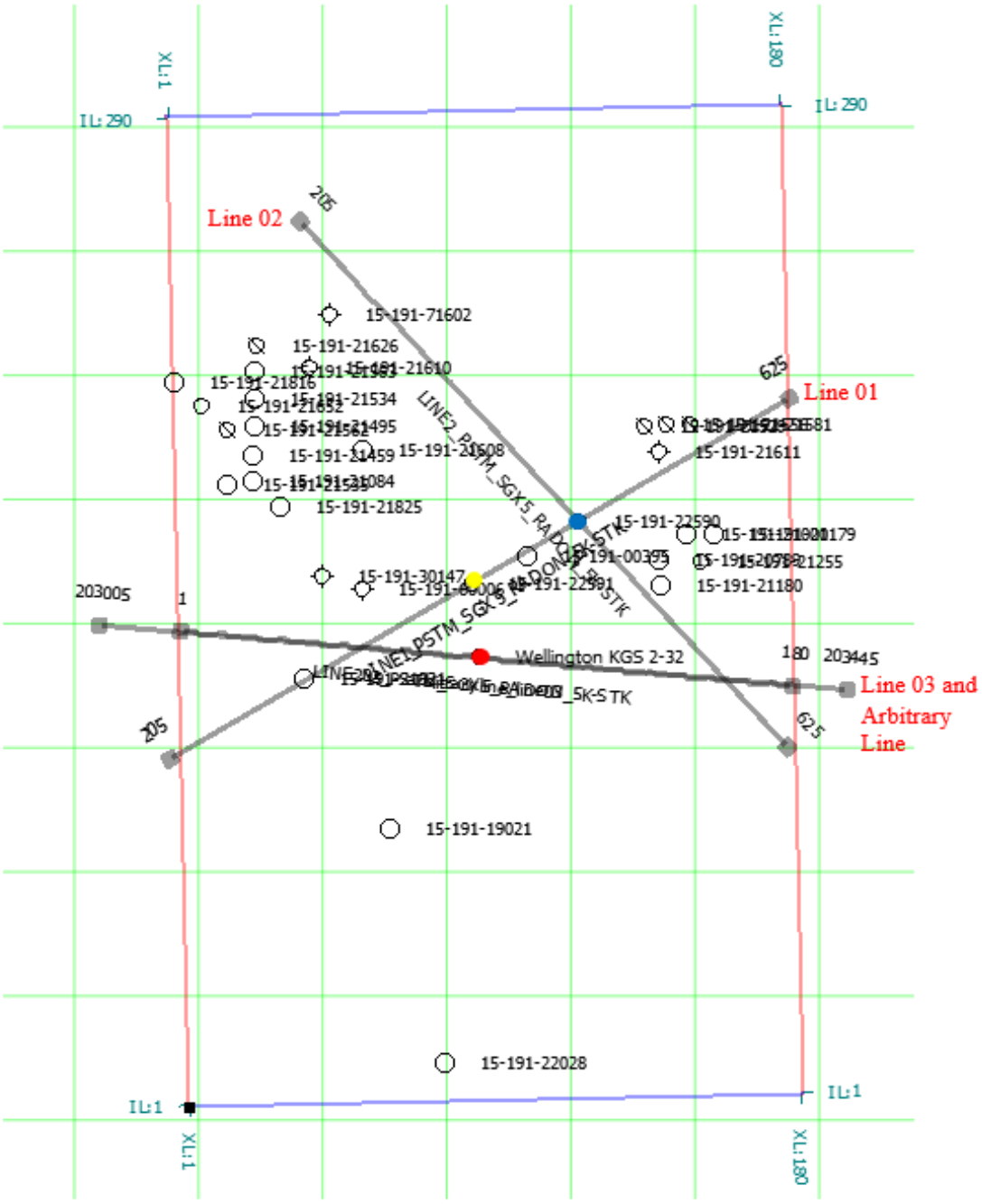

Figure 1.1.2. Base map of the field site with the outline of the pre-injection 3-D seismic survey displayed. The in-lines (1-290) are displayed from south to north, and the crosslines (1-180) displayed from west to east. The two pre-injection 2-D seismic lines (lines 01 and 02) and one post-injection 2-D seismic line (line 03) are also displayed. An arbitrary line, which directly overlays seismic line 03, was extracted from the 3-D seismic survey for time-lapse seismic analysis. The post-injection seismic line crosses through the Mississippian reservoir CO_2 injection well, KGS #2-32 (red). Wells KGS #1-28 (blue) and KGS #1-32 (yellow) are intersected by seismic lines 02 and 01, respectively. The 3-D seismic survey consists of 180 crosslines and 290 in-lines with a trace spacing of 25 meters by 25 meters. This map was generated in Hampson-Russell Software.

CHAPTER 2: GEOLOGICAL SETTING

Section 2.1 Field Site

Wellington field was discovered on December 4, 1929 in Sumner County, south-central Kansas, and covers an area of approximately 22.6 square kilometers (Figure 1.1.1). The primary producing horizons of Wellington field are the Mississippian (Osagean) and the Lansing-Kansas City reservoirs. Wellington field has produced more than 20.8 million cumulative barrels of oil from the Mississippian and Lansing-Kansas City reservoirs, as of August 2018, and currently has 55 active wells (Kansas Geological Survey website, 2018). In recent years, there has been a decline in production from Wellington field; therefore, a renewed interest in enhanced oil recovery of the field began in the 1990s (Montgomery et al., 1998).

Section 2.2 Geological Setting

In the midcontinent United States, Paleozoic chert reservoirs with complex pore systems are prolific hydrocarbon producers; a good example is the high porosity-low resistivity Lower Mississippian (Osagean) chert reservoirs found in northern Oklahoma and southern Kansas. In general, the Mississippian is composed of interbedded chert, dolomite, and limestone; however, the reservoir used in this study consists of chert and dolomite (Figure 2.2.1). Production from the Mississippian (Osagean) reservoirs in south-central Kansas primarily occurs along the flanks of the Central Kansas Uplift, with the greatest production within the Pratt Anticline (Figure 1.1.1). In addition, the Mississippian System lies beneath a major regional unconformity between the Mississippian and Pennsylvanian which creates a structural trap, a primary component for production (Colleary et al., 1997; Montgomery et al., 1998; Watney et al., 2001). According to Montgomery et al. (1998), these structural features began developing during the

Early Mississippian; therefore, they may have influenced the depositional setting of these reservoirs.

Osagean rocks were deposited on the carbonate shelf that extended over a large portion of the central and southwestern United States. During the Lower Mississippian age, southern Kansas was covered by the outer shelf and shelf margin (Figure 2.2.2). Deposited in transgressive-regressive cycles, the outer shelf facies are largely undolomotized, while principal facies on the shelf margin are comprised of sponge spiculitic wackestones to grainstones interbedded with shelf facies. These deposits exhibit a shallowing-upward succession due to the transgressive-regressive cycles (Watney et al., 2001). In addition, they exhibit evidence of having undergone a series of diagenetic events associated with post-Mississippian subaerial exposure (Montgomery et al., 1998; Watney et al., 2001) (Figure 2.2.3). All of this is overlain by the Pennsylvanian shales, creating the Pennsylvanian unconformity (Figure 2.2.4). Although early discovery of the Lower Mississippian (Osagean) reservoirs occurred in 1927, renewed interest in the reservoirs began in the 1990s for enhanced oil recovery (Montgomery et al., 1998).

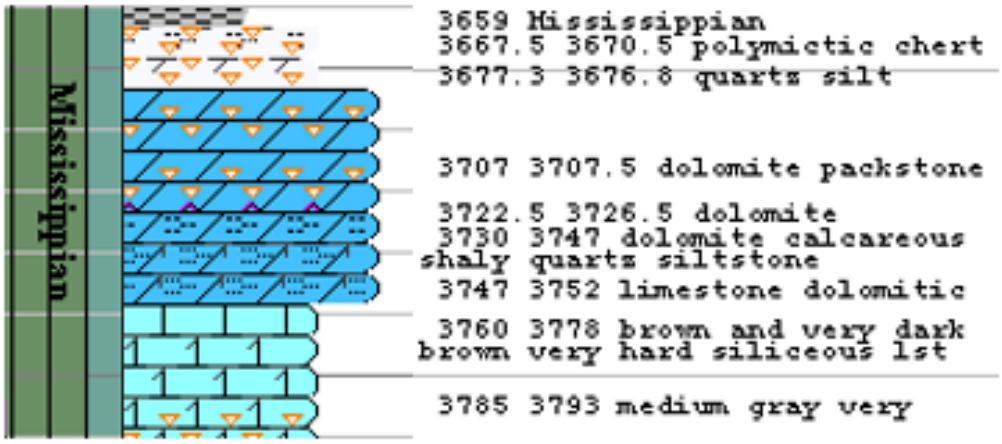

Figure 2.2.1. Rock column displaying the lithology for the Mississippian at KGS #2-32 with a description and depths (in feet) to the right. The white with orange triangles signifies chert, the dark blue models dolomite, and the light blue at the bottom represents limestone. KGS #2-32 is perforated from 3664-3706 feet (approximately from 1117-1130 meters). Modified from kgs.ku.edu.

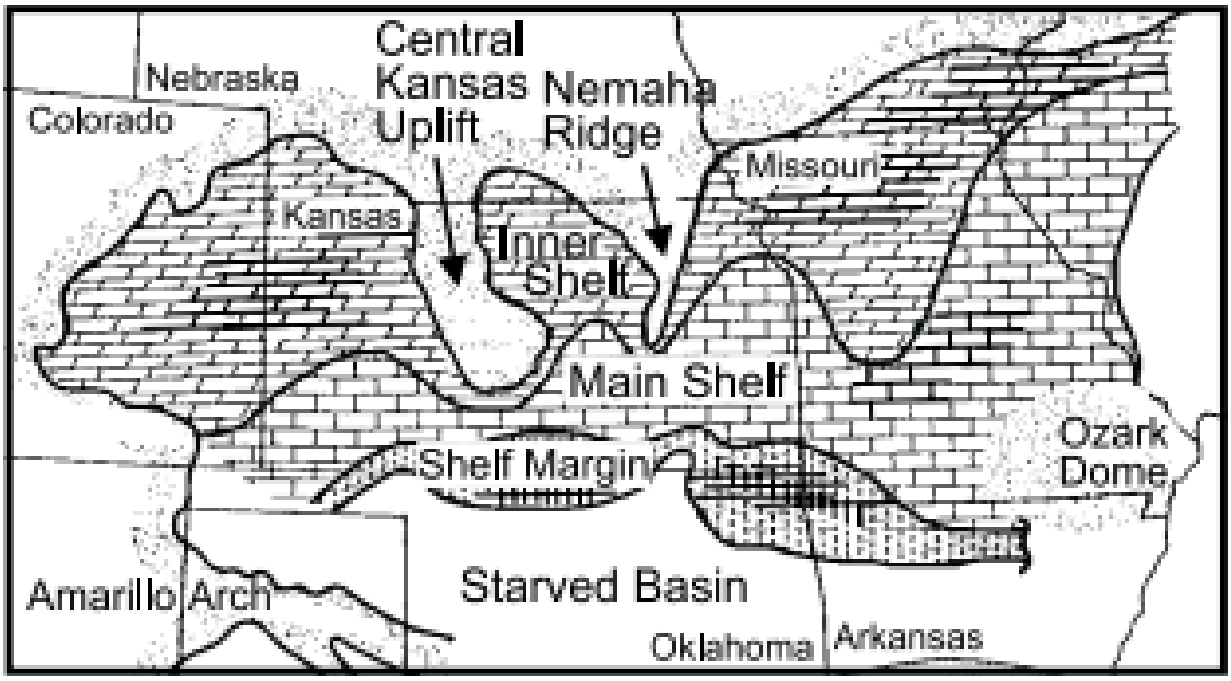

Figure 2.2.2. Paleogeographic map of the Midwest, specifically Kansas, and surrounding areas during the Osagean. It displays the shelf margin, basinal conditions, as well as, both the upper and lower shelves (Watney et al., 2001).

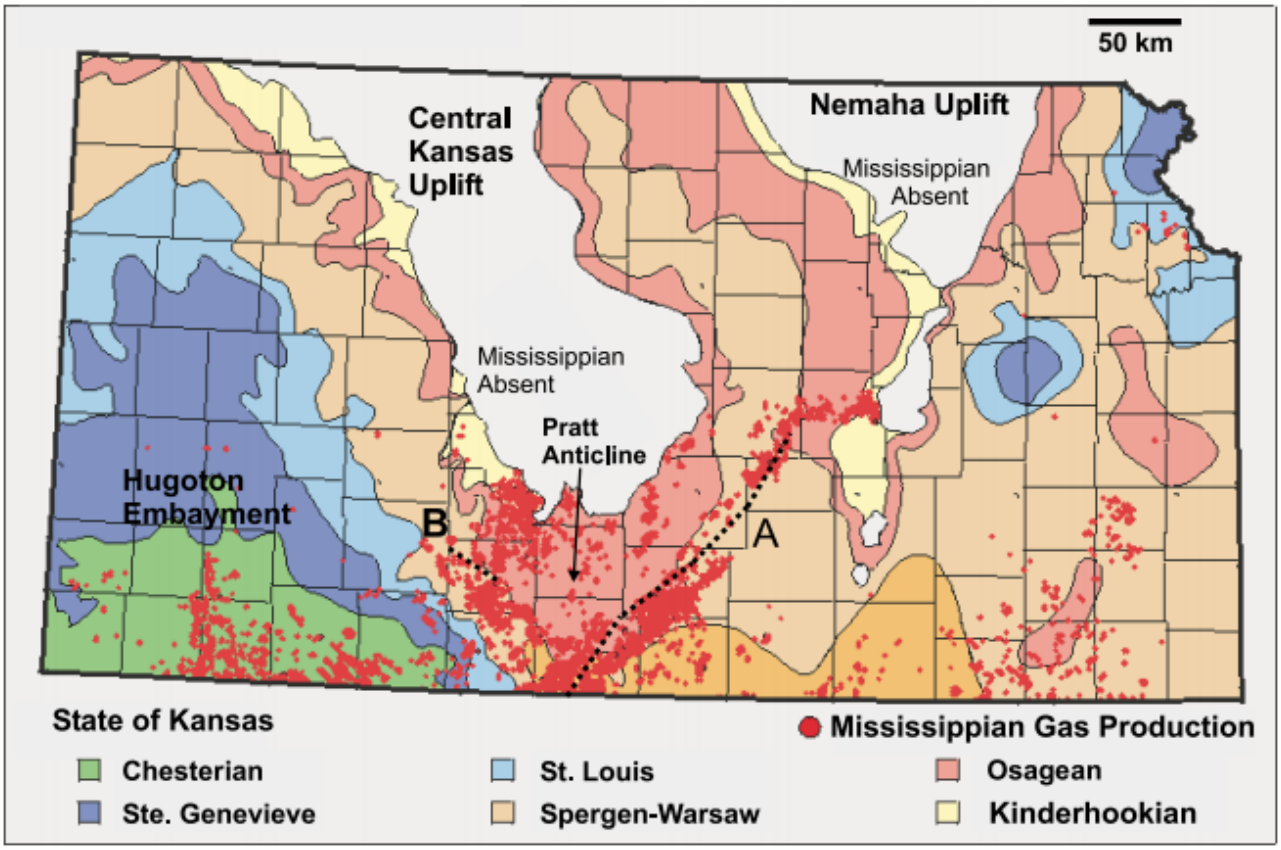

Figure 2.2.3. Map of pre-Pennsylvanian subcrop of Mississippian strata in Kansas with major structural features shown. The black dotted lines A and B are significant basement lineaments that are important to the chat formation (Watney et al., 2001).

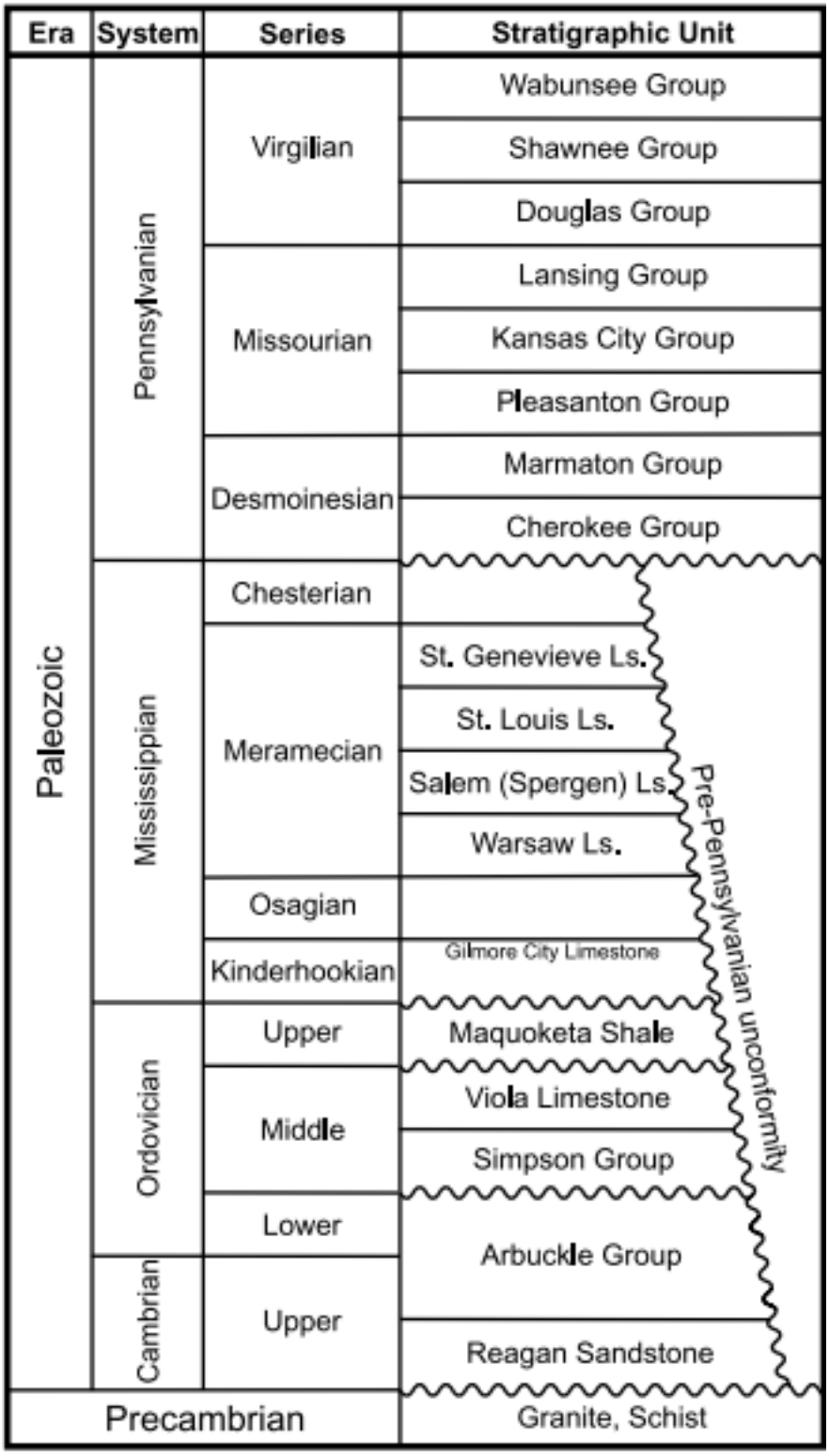

Figure 2.2.4. Stratigraphic chart of central Kansas displaying the pre-Pennsylvanian unconformity (Nissen et al., 2009).

CHAPTER 3: SEISMIC DATA AND POST-STACK ANALYSIS

3.1 Seismic Data

To monitor the CO_2 injection at Wellington field, two 2-D pre-injection seismic lines (line 01 and line 02) and a 3-D seismic survey were acquired in 2010 by Paragon Geophysical Services Inc., with a final 2-D seismic line (line 03) acquired post-injection in 2016. Seismic line 03 directly crosses through the injection well, KGS #2-32 (Figure 1.1.2). The pre-injection 3-D seismic survey consists of 180 crosslines and 290 in-lines with a trace spacing of 82.5 feet by 82.5 feet (25 meters by 25 meters). The post-injection 2-D seismic line consists of 440 CDP's (203005 to 203445) (Table 3.1.1). All seismic data is pre-stack time migrated and was initially processed from 2010-2011 by FairfieldNodal. In 2016, the seismic data was re-processed taking into consideration anisotropy for preservation of amplitudes. Re-processing of the seismic data ultimately resulted in noisier data but a more accurate relative amplitude (Kansas Geological Survey Data Release, 2016).

An arbitrary line, which directly overlaid the 2-D post-injection seismic line, was extracted from the 3-D pre-injection seismic survey for time-lapse seismic analysis and comparison with the 2-D post-injection seismic line. Time-lapse seismic analysis was inconclusive; therefore, I began to analyze the 2-D post-injection seismic gathers around the injection well, KGS #2-32 (CDP 203230), versus away from the injection site to identify differences possibly due to the introduction of CO_2. In addition, a synthetic seismogram was created for each 2-D seismic line and their respective wells. I achieved good agreement between synthetic and actual seismic data for the synthetic seismogram between seismic line 03 and KGS #2-32 with a maximum cross correlation of 0.551 (figure 3.1.1-figure 3.1.3).

3.2 Post-Stack Seismic Analysis

The majority of seismic analysis methods utilized in this study analyze the 2-D post-injection pre-stack seismic gathers; however, our first approach analyzed the 2-D post-injection post-stack seismic line and 3-D pre-injection post-stack seismic survey. Initially, we tried to image the CO_2 in the Mississippian reservoir by utilizing time-lapse seismic analysis. Time-lapse seismic analysis requires the re-acquisition of the same seismic survey/line over a period of time to visualize how the subsurface changed through time. Time-lapse seismic analysis has proven to be an effective monitoring technique on a wide range of CO_2 storage projects, primarily in clastic reservoirs. A previous case study by Ivanova et al. (2013) tested the ability of time-lapse seismic analysis to monitor a CO_2 injection at the Ketzin site in Germany. Through this method, results from the Ketzin site study have been interpreted as being caused by changes in the fluid saturations. Another case study in the central North Sea, Sleipner field, focuses on utilizing time-lapse seismic analysis to image a CO_2 plume in the Utsira Sand, a major saline aquifer. Although time-lapse seismic analysis was able to clearly image the CO_2 plume through sub-horizontal high amplitude reflections and a velocity pushdown, intra-reservoir shale layers could only be interpreted with CO_2 beneath them (Figure 3.2.1) (Arts et al, 2004; Chadwick et al., 2004).

Time-lapse seismic analysis is commonly used in CO_2 injection studies to identify changes over time within the subsurface that may be caused by the introduction of CO_2. Typically, repeat seismic surveys are acquired over a period of time; however, for our study, repeat seismic data was not acquired post-injection. While Paragon acquired two 2-D seismic lines and a 3-D seismic survey pre-injection, only one 2-D seismic line was acquired post-injection and it did not directly overlay the two pre-injection seismic lines; therefore, an arbitrary

line, which directly overlays the 2-D post-injection seismic line, was extracted from the pre-injection 3-D seismic survey (Figure 1.1.2). By comparing a line extracted from the 3-D dataset and the 2-D seismic line, we can see the differences in data quality between the two different types of data (Figures 3.2.2-3.2.3). As shown in figure 3.2.2, reflectors in the 2-D seismic line are less continuous than reflectors in the arbitrary line from 3-D seismic data. Therefore, our new approach primarily focuses on analysis and comparison along the post-injection 2-D seismic line. Further seismic modeling was integrated with well control to enhance seismic interpretation and imaging of the CO_2 plume.

Seismic Data	2D pre-stack time migrated gathers
Processing by FairfieldNodal	NMO Correction, Time Variant Scaling 500 ms, Mild Radon Filtering Applied, Trace Equalization
Bandpass Filter	6 – 120 Hz
Trace Length	3.0 seconds
Sample Rate	2.0 milliseconds
Offset Range	25.3 – 2112.3 meters (83 – 6930 feet)
Number of CDP's	442 (203003 – 203445)
CDP Interval	12.57 meters (41.25 feet)

Table 3.1.1. Overview of the parameters for the 2-D post-injection pre-stack time migrated seismic gathers used in all analyses.

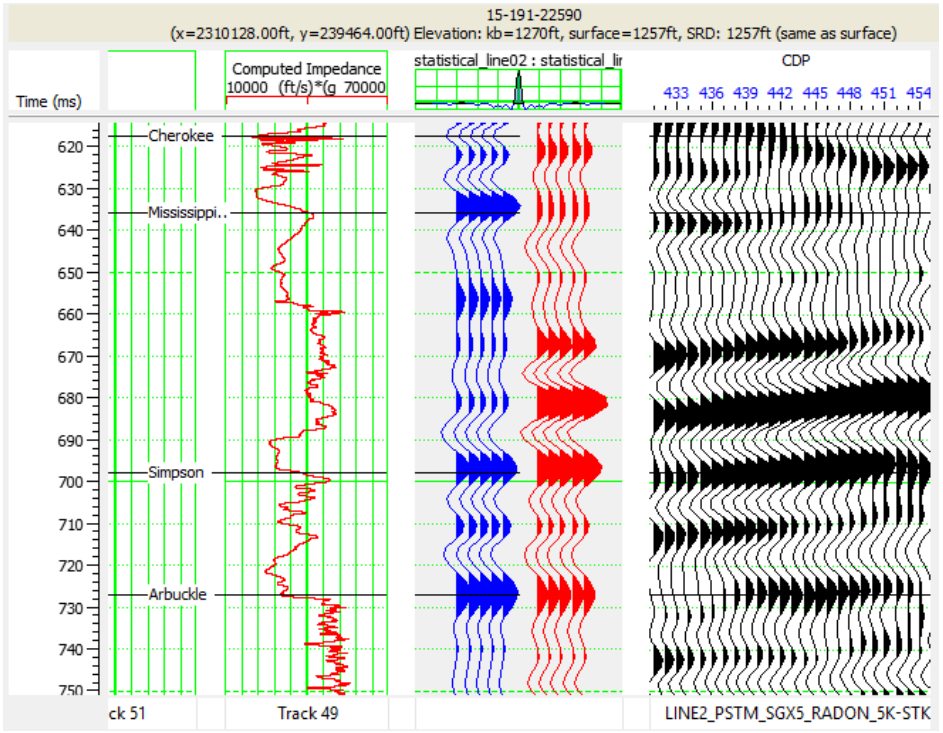

Figure 3.1.1. Synthetic seismogram for KGS #1-28 and seismic line 02. The synthetic seismic traces (blue) and actual seismic traces (red) display good agreement at KGS #1-28. The computed impedance curve for KGS #1-28 is displayed to the left with the tops for each horizon. Generated in Hampson-Russell Software.

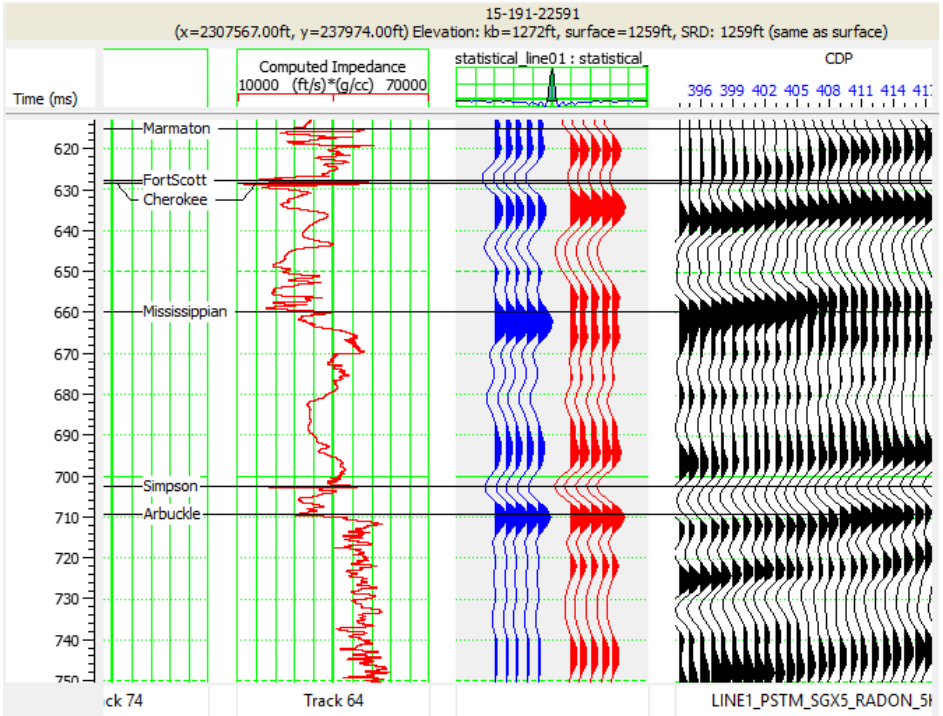

Figure 3.1.2. Synthetic seismogram for KGS #1-32 and seismic line 01. The synthetic seismic traces (blue) and actual seismic traces (red) display good agreement at KGS #1-32. The computed impedance curve for KGS #1-32 is displayed to the left with the tops for each horizon. Generated in Hampson-Russell Software.

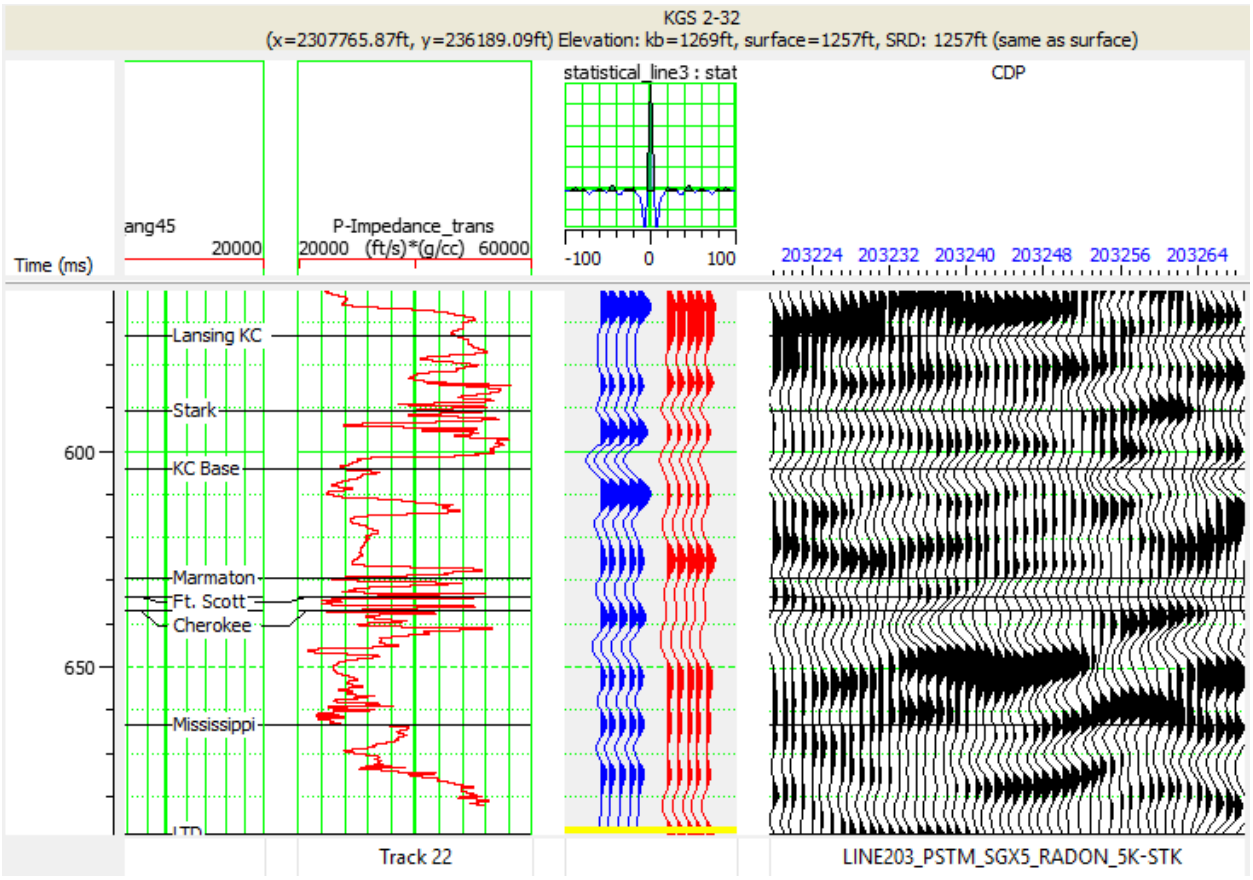

Figure 3.1.3. Synthetic seismogram for KGS #2-32 and seismic line 03. The synthetic seismic traces (blue) and actual seismic traces (red) display good agreement at KGS #2-32. The computed impedance curve for KGS #2-32 is displayed to the left with the tops for each horizon. Generated in Hampson-Russell Software.

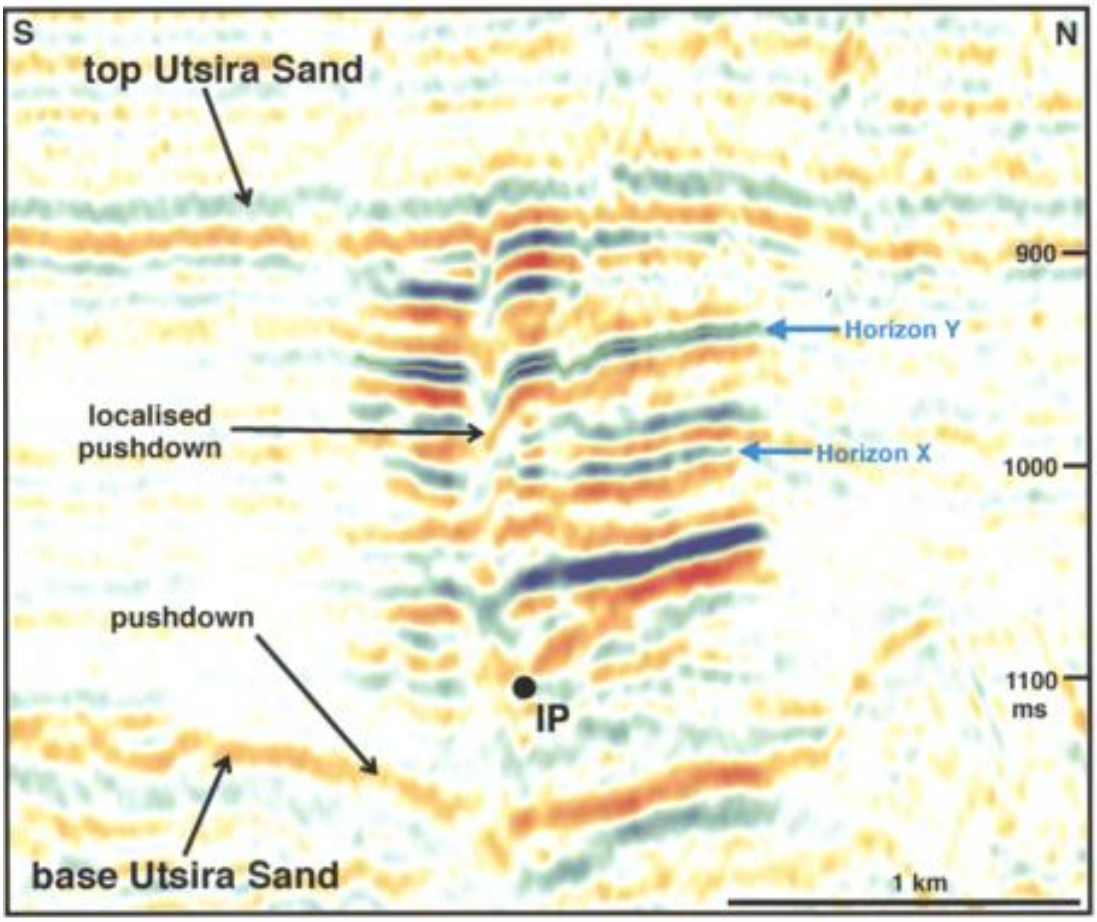

Figure 3.2.1. Seismic data acquired in 1999 (post-injection) of the Utsira sand, central North Sea. The primary velocity pushdown beneath the CO_2 is outlined at the base of the Utsira sand. IP is the approximate location of the injection point (corrected for the pushdown) (Chadwick et al., 2004).

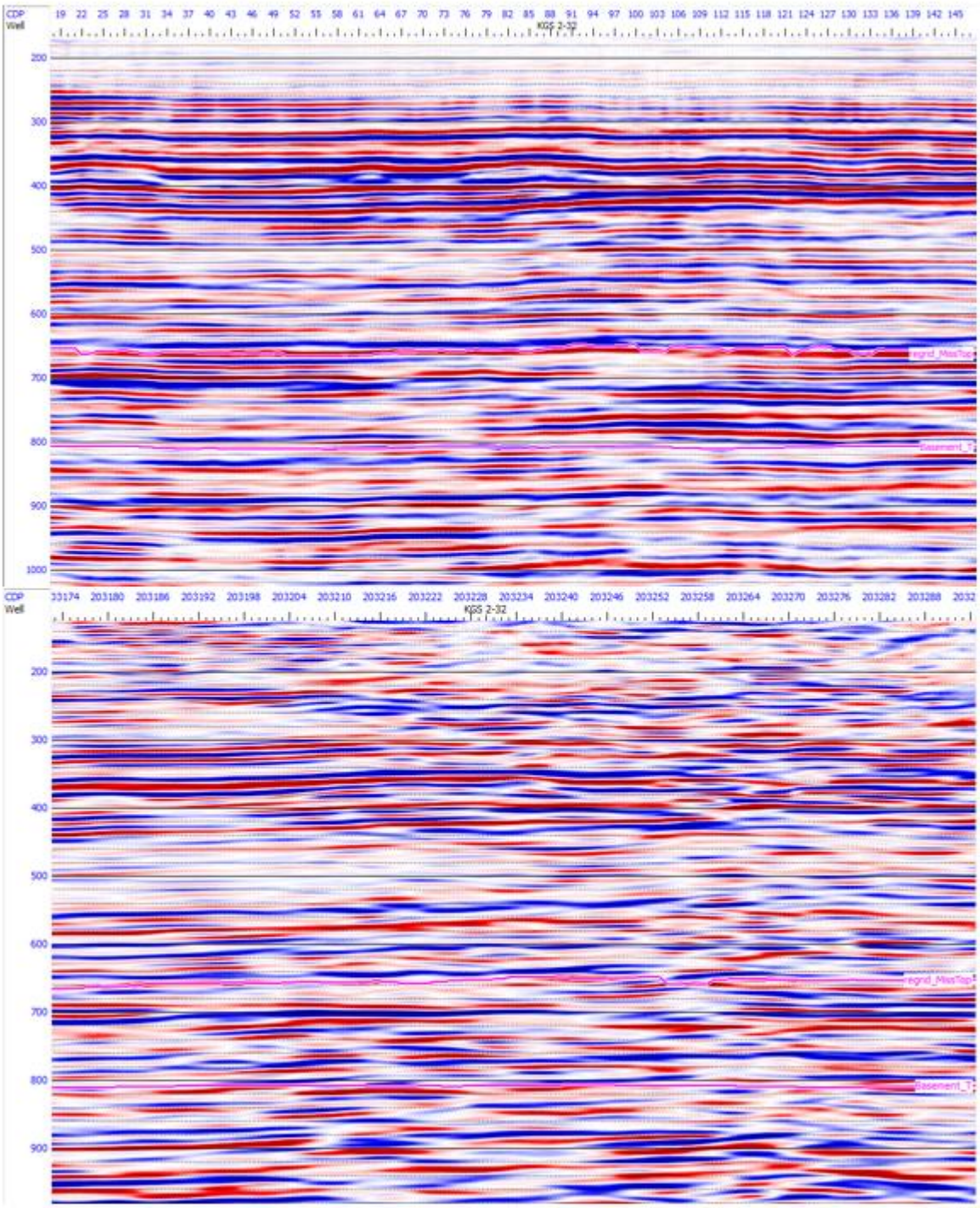

Figure 3.2.2. Comparison of the arbitrary line extracted from the pre-injection 3-D seismic survey (top) and the post-injection 2-D post-stack seismic line (bottom) did not present any significant amplitude changes. The comparison displays the difference in data quality between 2-D and 3-D seismic data. The primary horizons used in analysis are displayed in black, with the injection well also displayed. KGS #2-32 is displaying the p-wave curve. The seismic lines were displayed in Hampson-Russell Software.

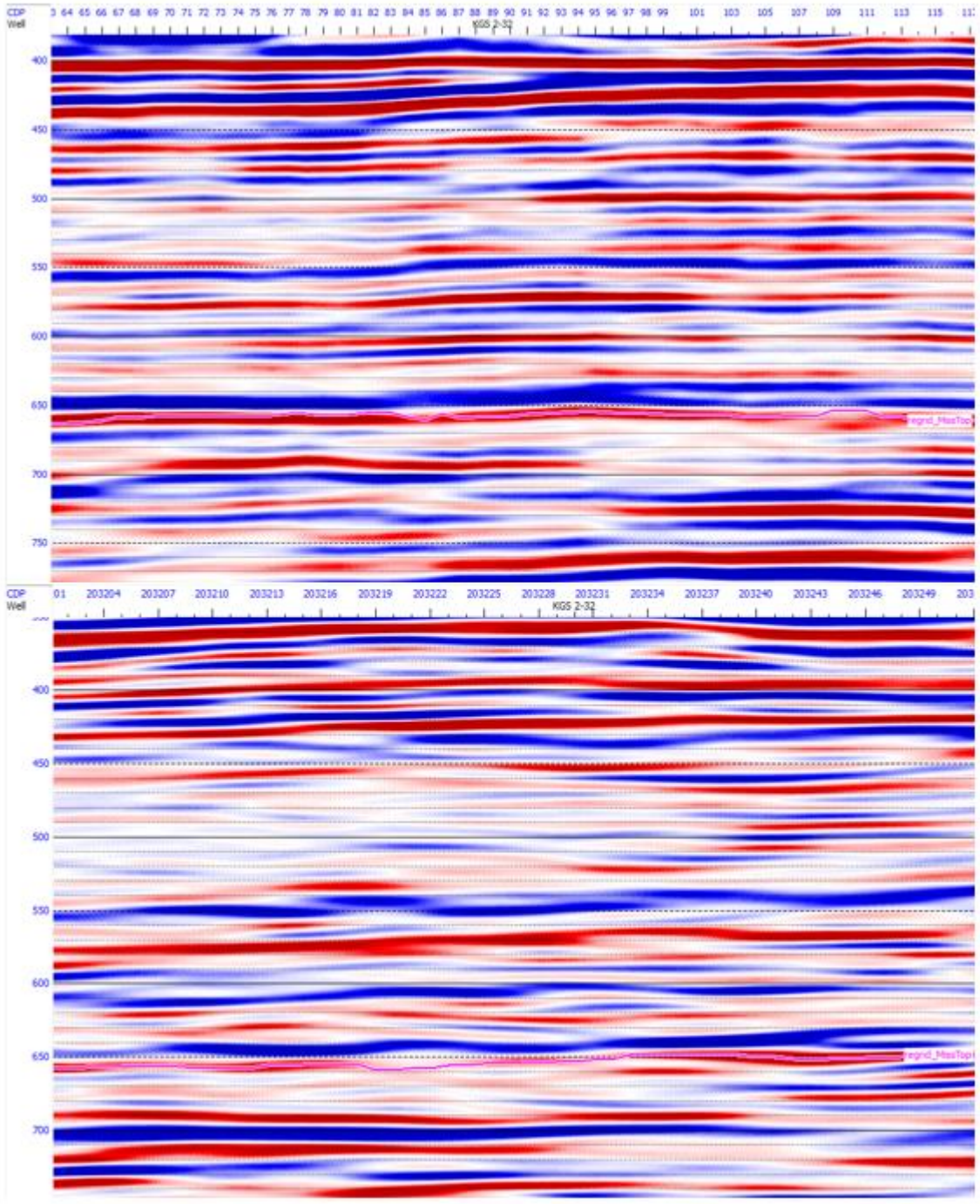

Figure 3.2.3. To better compare the arbitrary line and 2-D post-injection seismic data, I zoomed in on the area directly surrounding KGS #2-32 on both lines. The arbitrary line is on top and the location of KGS #2-32 is annotated at the top at CDP 89. The 2-D post-injection seismic line is on the bottom with the location of KGS #2-32 at CDP 203230. The Mississippian reservoir is displayed in magenta.

CHAPTER 4: FLUID SUBSTITUTION MODELING

Section 4.1 Fluid Substitution Modeling Background

As stated in section 3.2, our first approach to image the CO_2 within the Mississippian reservoir using time-lapse seismic analysis was inconclusive due to the differences between the quality of 2-D and 3-D seismic data; therefore, we changed our approach for imaging the CO_2 plume. Our second approach to image the CO_2 within the Mississippian reservoir includes analysis of the 2-D post-injection seismic gathers near and far from the injection site to identify any changes possibly introduced by the presence of CO_2. Seismic analysis methods utilized include fluid substitution modeling and Amplitude Variation with Offset (AVO) analysis.

Fluid substitution modeling was the first seismic analysis method utilized in our new approach to assess the feasibility of imaging the CO_2 in the Mississippian reservoir. Fluid substitution modeling is a tool used for modeling the various possible fluid scenarios at an injection point to determine how introducing a fluid (i.e. CO_2) into the subsurface affects seismic velocities and impedances, and identify possible observed AVO anomalies (Smith et al., 2003; Arts et al., 2004). There are two main types of fluid substitution modeling considered in this study: Gassmann and Patchy (Adam et al., 2006; Vega et al., 2007). While Patchy fluid substitution models are believed to provide a better fit in CO_2/water systems, we evaluate both Patchy and Gassmann models because Gassmann models have a firmer theoretical footing (Altundas et al., 2013). Gassmann's theory is commonly applied to predict the bulk modulus for rocks saturated with different fluids (Adam et al., 2006). Gassmann's theory relates the bulk modulus of a rock to its pore, frame, and fluid properties through equation 1 (stated below) (Smith et al., 2003).

$$K_{sat} = K_{dry} + \frac{(1-\frac{K_{dry}}{K_{min}})^2}{\frac{\varphi}{K_{fl}}+\frac{1-\varphi}{K_{min}}-\frac{K_{dry}}{K^2_{min}}}. \qquad (1)$$

The variables in Gassmann's equation are well constrained or can be directly measured. Gassmann's theory estimates the saturated bulk modulus (K_{sat}) by utilizing the bulk moduli of the dry rock (K_{dry}), fluid (K_{fl}), and forming minerals (K_{min}), as well as, the rock porosity (ϕ) (Adam et al., 2006; Arts et al., 2004). It is also based on five primary assumptions for a porous system; the assumptions are

1. Pore pressure between pores is in equilibrium,
2. The porous frame is made up of a single, solid material,
3. It is a closed system,
4. Pores are homogeneously filled with a non-viscous fluid, and
5. The solid frame is not chemically influenced by the pore fluid.

In addition, although a constant shear rock modulus is implied, it is an outcome of Gassmann's theory instead of an assumption (Adam et al., 2006). Gassmann's theory assumes a homogeneous rock, therefore Patchy fluid substitution modeling is commonly believed to be a better fit for CO_2/H_2O saturated carbonate rocks; however, both are tested throughout this study and in prior investigations by Graham et al. (2016).

In 2016, Graham et al. investigated the effects of Gassmann and Patchy fluid substitution on CO_2 saturation in the Mississippian reservoir. Simulations were completed using 0% CO_2 saturation and 100% H_2O saturation up to 100% CO_2 saturation with 0% H_20 saturation in increments of 2%. During simulations, oil saturation was not taken into account. In addition, Graham et al. (2016) completed these simulations using both Gassmann and Patchy fluid substitution modeling to identify which model better fit the Mississippian reservoir. Their

findings concluded up to a 10% change in reflectivity with the introduction of CO_2 in the Mississippian chert reservoir (Figure 4.1.1). In addition, Gassmann and Patchy models were used to model Amplitude Variation with Offset (0-45°) and CO_2 saturation within the Mississippian and Arbuckle reservoirs. Specifically, in the Mississippian reservoir, both models display a decrease in amplitude with an increasing angle of incidence and CO_2 saturation (Figure 4.1.2). According to their simulations, the Gassmann model will provide higher resolution for CO_2 saturations between 2-10%, as typically observed in clastic and less consolidated reservoirs, while the Patchy model provides a more linear response to CO_2 saturation changes. Our modeling primarily focuses on Patchy modeling which is representative of more consolidated, incompressible reservoirs like carbonates.

4.2 Fluid Substitution Modeling Analysis

Our approach included analysis of the post-injection 2-D seismic line near and away from KGS #2-32 to identify any changes possibly introduced by the presence of CO_2. The location of well KGS #2-32 in relation to seismic line 03 is displayed in figure 1.1.2. Fluid substitution modeling of the 2-D post-injection seismic line was completed using Hampson-Russell Software and requires p-wave, s-wave, and density logs. All models were compared to the original well logs for KGS #2-32. The zone of interest for all models was from 3655 to 3775 feet (1,114 to 1,150 meters) to encompass the entire Mississippian reservoir. As stated in section 4.1, fluid substitution modeling is commonly used to model the effects on the subsurface due to the introduction of a fluid (CO_2 in our study). Post-injection CO_2 saturations were calculated by Eugene Holubnyak (personal communication, 2017) and could be up to 50% in some areas; however, the average saturation around the injection site is approximately 25% and dissipates

away from the well (Figure 4.2.1). Fluid substitution models were simulated utilizing 10%, 25%, and 50% CO_2 saturations to display the effects of the dominant saturation and the extremes of the CO_2 saturation range. The parameters used for in-situ and post-injection saturations are displayed in table 4.2.1. Except for the saturation percent of each fluid, the fluid parameters and petrophysical parameters remained constant throughout each model. The input petrophysical parameters for the matrix are displayed in table 4.2.2. As expected, each model displayed a decrease in normal incidence acoustic impedance with a larger decrease correlating to higher CO_2 saturations (Figure 4.2.2). The change in acoustic impedance within the Mississippian reservoir for each model was calculated in Microsoft Excel utilizing values exported from Hampson-Russell Software. Calculations concluded the possibility of up to a 6.07% decrease in acoustic impedance with 25% CO_2 saturation and up to a 13.33% decrease in impedance with 50% CO_2 substitution. In addition, synthetics were generated at the location of KGS #2-32 for all three CO_2 saturations to determine if there was a change in amplitude with increasing saturations (Figure 4.2.3). The synthetics were overlain in Matlab and generally display an increase in amplitude with increasing CO_2 saturation. These results were supplemented with AVO analysis.

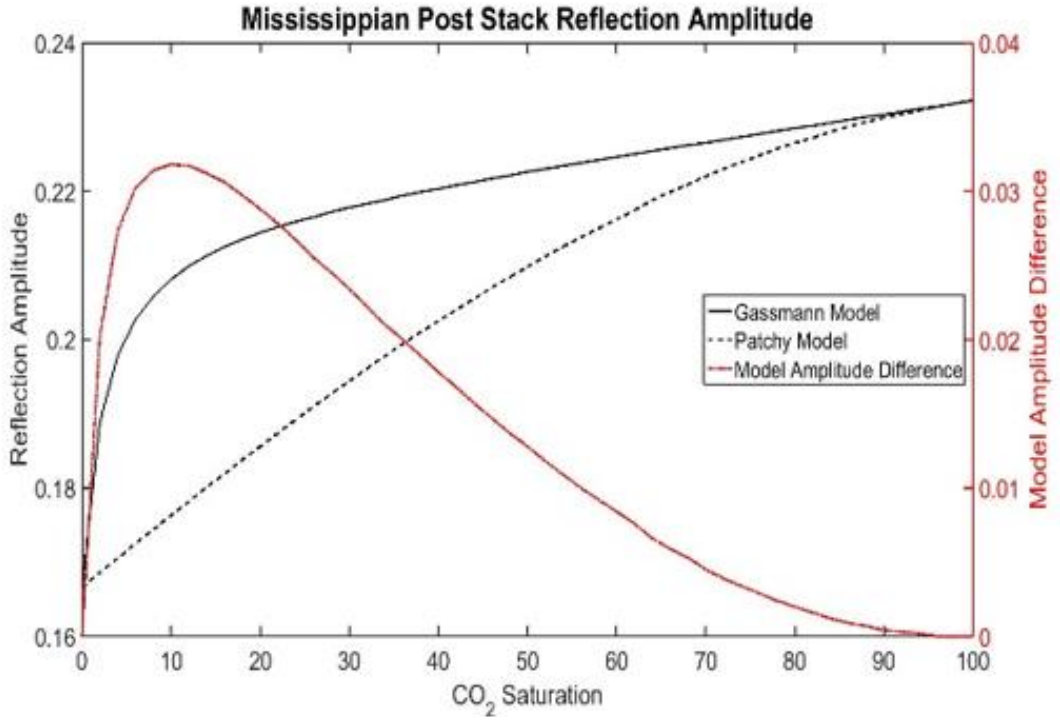

Figure 4.1.4. Gassmann and Patchy reflection amplitude models for the Mississippian reservoir generated by Graham et al. (2016). He also modeled the difference of CO_2 saturation between these two models.

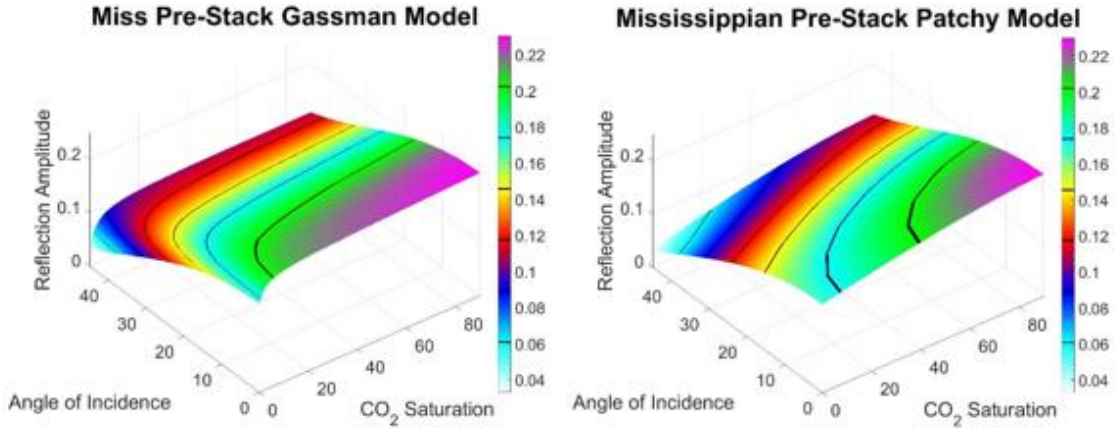

Figure 4.1.5. Pre-stack synthetic Gassmann and Patchy models generated by Graham et al. (2016). These models display a decreasing amplitude with increasing angle of incidence and CO2 saturation. The black lines are amplitude contours and the color scale indicates the model cell saturation value percent.

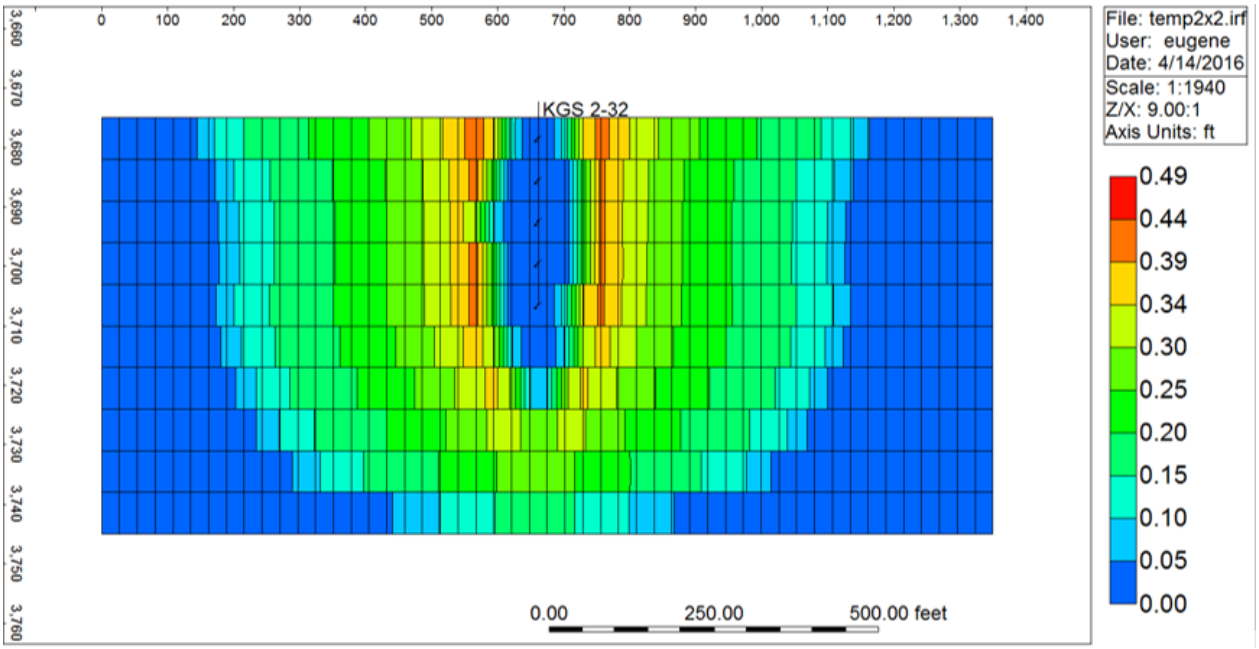

Figure 4.2.1. CO_2 saturation modeled around well KGS #2-32, modeled by Eugene Holubnyak (2017 personal communication). It can be difficult to project precise CO_2 saturation around the injection site. In some areas, saturation can be as high as 50% but could be difficult to detect in others. The color scale indicates the model cell saturation value percent.

Reservoir Parameters			
	Parameter	In-situ	Post-injection
Brine	Density	1.09 g/cc	1.09 g/cc
	Bulk Modulus	2.38 GPa	2.38 GPa
	% Present	76%	56%
Oil	Density	0.805 g/cc	0.805 g/cc
	Bulk Modulus	1 GPa	1 GPa
	% Present	24%	19%
CO_2	Density	0.3 g/cc	0.3 g/cc
	Bulk Modulus	0.05 GPa	0.05 GPa
	% Present	0%	25%

Table 4.2.1. The in-situ values and post-injection values used for fluid substitution modeling are displayed. The post-injection values used for brine and oil were calculated assuming the same ratio existed post-injection. 25% was the average CO_2 saturation around the injection well based on numbers calculated by Eugene Holubnyak (personal communication, 2017).

Rock Matrix Parameters			
Mineral	Dolomite 50%	Quartz 40%	Calcite 10%
Density	2.87 g/cc	2.65 g/cc	2.71 g/cc
Bulk Modulus	94.9 GPa	36.6 GPa	76.8 GPa
Shear Modulus	45 GPa	45 GPa	32 GPa

Table 4.2.2. Parameters used in fluid substitution for the rock matrix of the Mississippian reservoir. The percentage of each mineral in the rock matrix is from Graham et al. (2016).

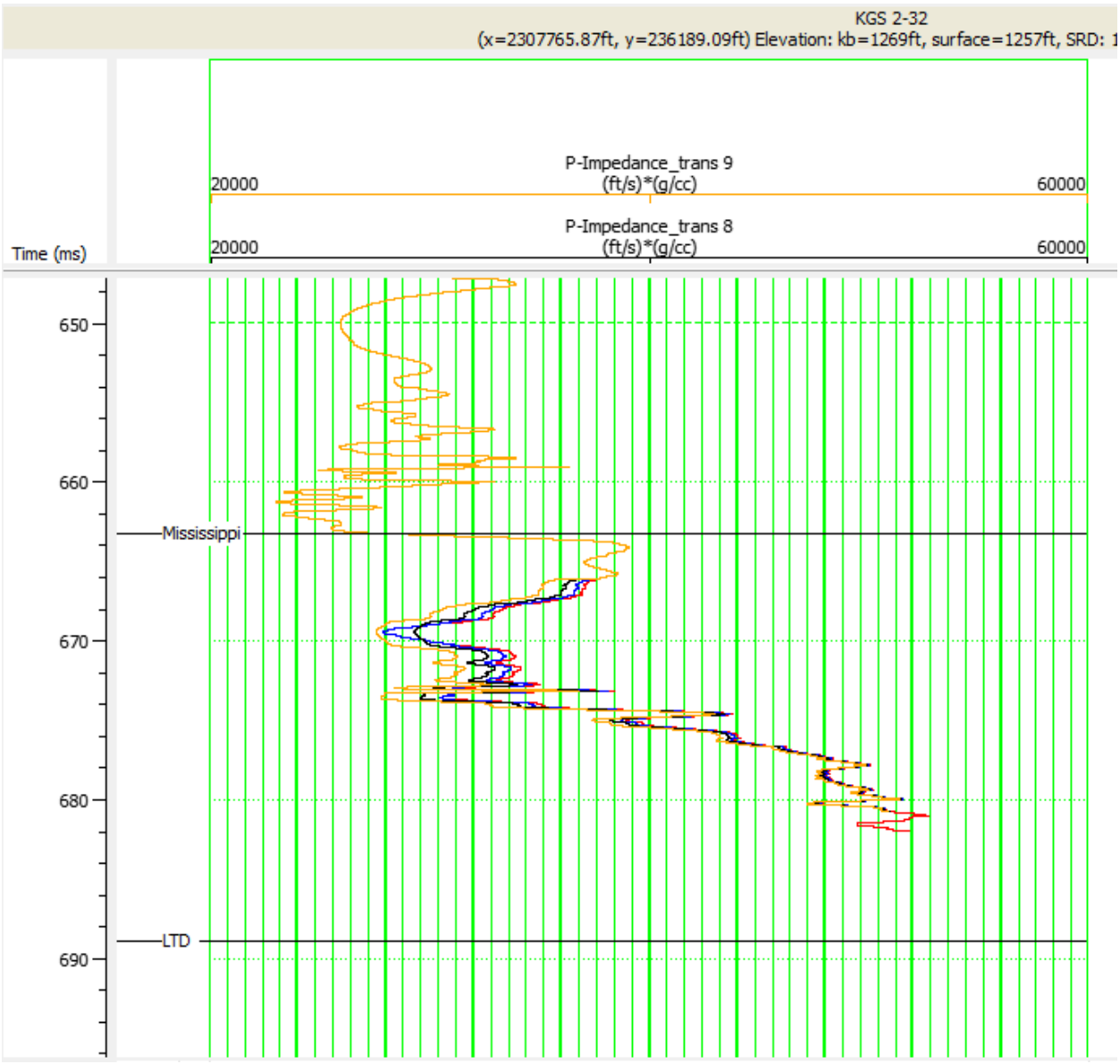

Figure 4.2.2. Well curve from KGS #2-32 displaying the initial impedance (red curve), the acoustic impedance with 10% CO_2 saturation (blue curve), the acoustic impedance with 25% CO_2 saturation (black curve), and the acoustic impedance with 50% CO_2 saturation (yellow curve). These three curves show a decrease in normal incidence acoustic impedance with increasing CO_2 saturation. With 10% CO_2 saturation, the acoustic impedance curve exhibits an average decrease of 0.71% over the reservoir interval and up to a 2.35% change. The acoustic impedance curve for 25% CO_2 saturation displays an average decrease of 1.83% and a maximum decrease of 6.07%. Finally, with 50% CO_2 saturation, the acoustic impedance has an average decrease of 4.64% with a maximum decrease of 13.33%. All curves were generated in Hampson-Russell Software.

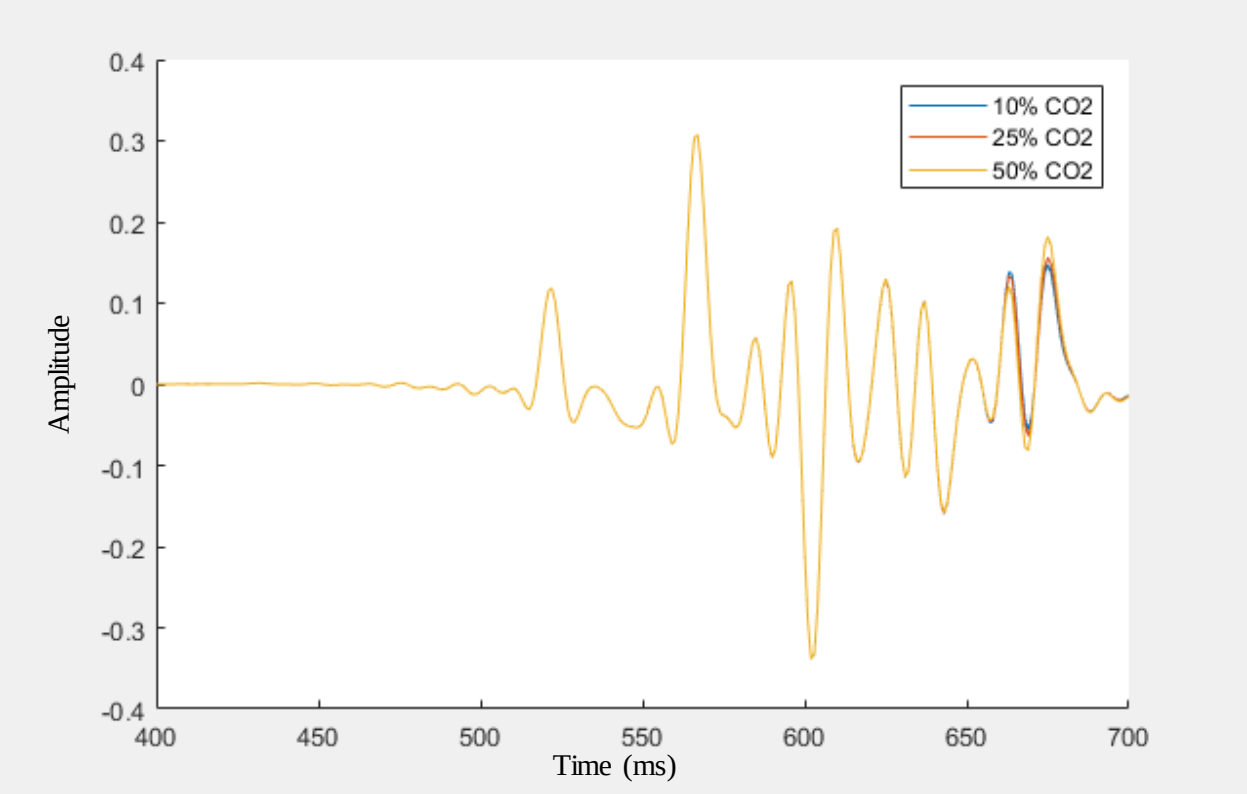

Figure 4.2.6. The synthetics for each CO_2 saturation were overlain in Matlab to analyze the change in amplitude with increasing saturations. The zone of interest is from approximately 650-680 ms and displays an increase in amplitude with increasing CO_2 saturation.

CHAPTER 5: AMPLITUDE VARIATION WITH OFFSET

Section 5.1 Amplitude Variation with Offset Background

Utilizing Hampson-Russell Software Geoview module, the standard amplitude variation with offset (AVO) attributes, intercept (A) and gradient (B), were analyzed at the Mississippian reservoir in Wellington field. The AVO intercept is the measure of the normal incidence amplitude (or seismic reflectivity), while the AVO gradient measures amplitude change with offset (or angle of incidence) (Castagna and Swan, 1997). Intercept and gradient are crossplotted to derive hydrocarbon indicators from the seismic data. AVO intercept is on the x-axis with AVO gradient on the y-axis of the crossplot. Each crossplot exhibits a background trend which directly passes through the origin and typically has a negative slope, although it can be positive at extremely high V_P/V_S ratios (Figure 5.1.1). Oftentimes, a well-defined background trend is evidence of brine-bearing clastic rocks (Castagna and Swan, 1997; Castagna et al., 1998). Any deviations from the background trend are highly indicative of hydrocarbons or unusual lithologies. Aside from being utilized to identify hydrocarbons, A-B crossplots can also be used to indicate CO_2 saturation (Castagna et al., 1998), although it is difficult to quantify changes in CO_2 saturation in the majority of reservoirs (Brown et al., 2007).

There are four classifications of AVO anomalies present on A-B crossplots. Initially, Rutherford and Williams (1989) identified only three classifications of AVO anomalies; however, Castagna et al. (1998) later divided Class III anomalies into two different classifications to create four. AVO behavior classifications identify the change in impedance between the overlying unit and the zone of interest. To classify the AVO behavior of the zone of interest, we look at the intercept and gradient. Each AVO class exhibits particular identifying

features to aid in determining which classification each anomaly is. This is further explained in Table 5.1.1 (Castagna and Swan., 1997; Castagna et al., 1998).

As shown through previous case studies, AVO analysis is a common technique used to monitor a CO_2 injection. One major field site where this technique has been tested was the Ketzin site in Germany, in which Ivanova et al. (2013) validated the use of analyzing the AVO response to monitor CO_2 storage in a sandstone reservoir. In 2007, Ivanova et al. (2013) drilled three boreholes (an injection well and two observational wells) to a depth of approximately 800 meters and utilized multiple repeat surveys to sufficiently analyze the area and the CO_2 injection. As of May 2013, over 64,000 tons of CO_2 had been injected into the reservoir. With the comparison of the first repeat survey and the baseline survey they were not able to differentiate between pore-pressure and CO_2 saturation related effects; however, they expect to be able to with the second repeat survey as the CO_2 saturation should be significantly higher. Through the integration of seismic modeling and petrophysical experiments, they were able to estimate the effect of CO_2 saturation on the AVO response on the seismic data. These techniques were more successful in monitoring CO_2 at the Ketzin site than in the Mississippian reservoir. At the Ketzin site, three times more CO_2 was injected compared to the Mississippian reservoir in this study. Also, the Ketzin study targeted a clastic reservoir instead of a carbonate reservoir like this study (Ivanova et al., 2013).

In 2015, Fadolalkarem analyzed the pre-injection 3-D pre- and post-stack seismic data with the initial processing from FairfieldNodal. Pre-stack angle gathers were utilized for AVO response classification of the reservoir. Similar to our research, they analyzed the A-B crossplots for the Mississippian reservoir at multiple locations. Initially, their seismic gathers at KGS #1-32 presented a Class III AVO response while the synthetic seismic gathers exhibited a Class IV

AVO response. Therefore, further processing was applied to the actual seismic gathers to remove linear coherent noise, and any distortions and artifacts introduced through seismic processing, similar to Appendices A-C in this thesis. After these processing steps were applied, the AVO response exhibited by the actual gathers matched the response given by the synthetic seismic gathers (Figure 5.1.2). In addition, the location of the A-B crossplot at the Mississippian reservoir was plotted for 11 wells located throughout the seismic survey and consistently observed a Class IV AVO response; however, his data is reverse polarity, therefore it is more likely a Class I AVO response (Fadolalkarem, 2015). Based on this study, it is reasonable that we should expect a Class I AVO response in the Mississippian reservoir with normal polarity at Wellington field.

Section 5.2 Amplitude Variation with Offset Analysis

Standard AVO attributes, intercept (A) and gradient (B), were analyzed at the Mississippian reservoir in Wellington field. Primary analysis occurred along the 2-D post-injection seismic line with f-k filtering (refer to Appendix A) applied and focused on changes in the AVO analysis near and far from the injection well, KGS #2-32. A-B crossplots and gradient curves were the primary source of analysis. All curves and crossplots were generated using Hampson-Russell Software version 10. Although multiple Common Depth Point (CDP) locations are analyzed, the seismic line and the majority of the input parameters remain constant throughout. A time window from 0 to 900 milliseconds (ms) was used for all analyses because everything below 900 ms is basement. In addition, the entire range of offsets was used for analysis, and the velocity field was computed using a single well (KGS #2-32) and log curve

(p_wave_1) (Figure 5.2.1). For all AVO analyses, the event picked was the Mississippian reservoir at approximately 3640 feet measured depth corresponding to 660 milliseconds.

The seismic line utilized in AVO analysis was the 2-D post-injection post-stack seismic data with f-k filtering applied. Before AVO analysis could be completed, more seismic processing was done to remove noise from the gathers. Further processing included creating and applying an f-k filter (Appendix A), trim statics (Appendix B), and AVO Offset Scaling (Appendix C). The f-k filter helped to remove noise in the far offsets and aided in the AVO response analysis. To identify any possible changes caused by the introduction of CO_2 into the reservoir, I compared the gradient curves and crossplots for CDP's near and far from the injection site along the same seismic line. The primary CDP's included in this study were 203070, 203123, 203230 (location of the injection well), 203325 and 203370 (Figure 5.2.2). I chose CDP's 203070 and 203370 because they are near the end of each side of the seismic line (far from the injection site CDP 203230) and therefore are not expected to contain any CO2, as well as, CDP's 203123 and 203325 because they are on either side of the injection well but closer to the injection site (Figure 5.2.2). The CDP's located on the left of the injection well (203070 and 203123, Figures 5.2.4-5.2.5) have higher normal incidence amplitudes (2.2 and 2.1) whereas the CDP's located to the right of the injection well (203325 and 203370, Figures 5.2.6-5.2.7) exhibit lower normal incidence amplitudes (1.1 and 1.1). CDP's away from the injection well exhibit greater amplitude scatter. In addition, the CDP's on the left exhibit a decrease in amplitude with increasing offset (gradient -3.6 and -2.1), while the CDP's on the right display an increase in amplitude with increasing offset (gradient 2.3 and 3.7) (up to 4,000 feet offset) (Figures 5.2.4-5.2.7). The gradient curve for CDP 203230 (location of KGS #2-32 and known location of CO_2 presence) displays less scatter than the CDP's surrounding and on either end of

the seismic line (Figure 5.2.3). In addition, all five primary CDP's display a sinusoidal shape in the gradient curve (Figures 5.2.3-5.2.7). All gathers examined exhibit an abrupt change in amplitude trend giving the amplitude variability a sinusoidal shape. To try to identify the cause of the sinusoidal shape, I analyzed the gradient curves for every fifth CDP along the f-k filtered 2-D post-injection seismic line; however, I used CDP's 203070, 203123, 203230, 203325 and 203370 for primary AVO analysis. The majority of the CDP's analyzed also exhibited either a sinusoidal shape or large data scatter (Figures 5.2.4-5.2.7). In addition, a common trend observed throughout the seismic line (every 5th CDP was analyzed) is a consistent AVO response to an offset of approximately 4,000-5,000 feet (1,219-1,524 meters). Next, I analyzed the gradient curves for the 2-D post-injection seismic line with different levels of processing applied. Once again, the gradient curves displayed a sinusoidal shape; therefore, we can conclude that the sinusoidal shape was not introduced through data processing. Finally, I analyzed the gradient curve for CDP 203230 in the angle domain (Figure 5.2.8). The sinusoidal shape is present in this curve as well and displays consistent AVO response up to approximately 37 degrees, which is expected as we reach the critical angle due to the limitations and assumptions of the Zoeppritz equations (Chopra and Castagna, 2014). As shown in figure 5.2.9, the 2-D post-injection seismic gathers at the Mississippian in KGS #2-32 exhibit angles of incidence up to 80 degrees which is well beyond critical angles. This follows the expectations of Zoeppritz equations (Figure 5.2.10). Therefore, the sinusoidal shape present in the majority of AVO gradient curves throughout the 2-D post-injection seismic line is due to post critical mode conversion. AVO analysis of this data should consider CDP angles of incidence up to a maximum of 40 degrees or approximately 4,000 feet of offset where the abrupt change in amplitude is observed.

The next step of AVO analysis was to analyze the crossplots for deviations from the background trend. Typically, the background trend has a negative slope and passes through the origin, and any deviations from it are indicative of hydrocarbons and/or unusual lithologies (Castagna and Swan, 1997; Castagna et al., 1998). The Mississippian reservoir reflection was plotted on the A-B crossplot in quadrant IV, which is typically the quadrant for a Class I AVO anomaly (Figure 5.2.11). In addition, it was characterized as a positive intercept (A) and negative gradient (B) which is also indicative of a Class I AVO response. When a unit is classified as a Class I AVO anomaly, they exhibit a higher impedance than the overlying unit and the reflection magnitude decreases with offset (Castagna et al., 1998). While this is useful information, the A-B crossplot was too scattered to be able to be reliable enough to identify changes in CO_2 saturation, although the data consistently indicates a Class I AVO response for the Mississippian reservoir. The gradient curves surrounding the injection well show changes in trend, which may be attributed to the introduction of CO_2. These results support the results from Fadolalkarem (2015) in which the Mississippian reservoir exhibits a Class IV AVO response; however, his data was reverse polarity, therefore we should expect a Class I AVO anomaly as shown in figure 5.2.11 (refer to section 5.1).

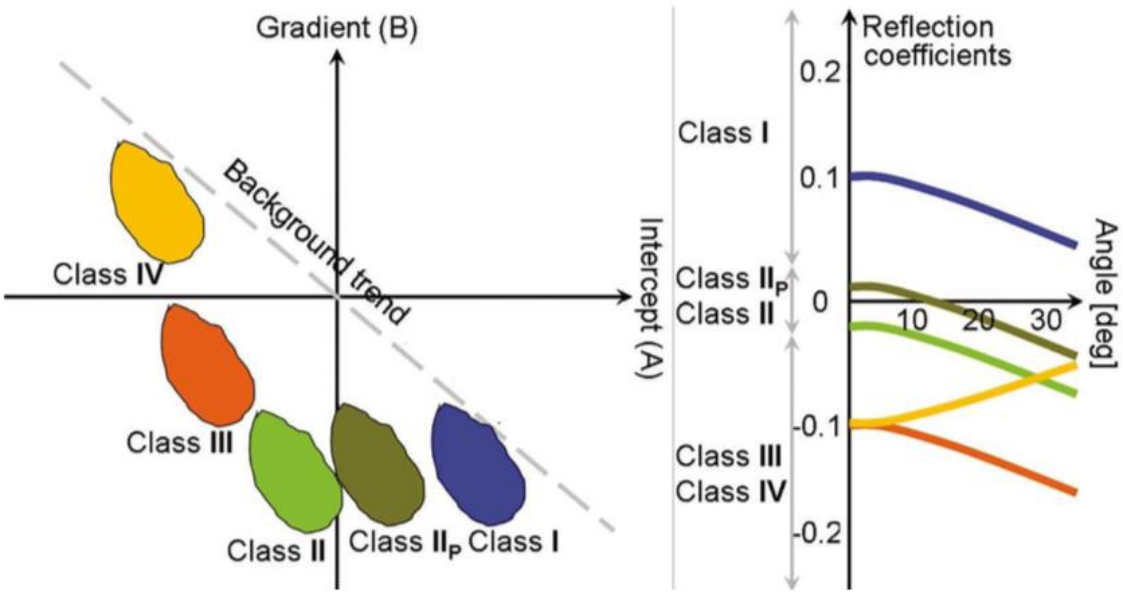

Figure 5.1.1. The background trend is displayed on an AVO crossplot along with the typical location of each AVO response class (Avseth et al., 2005; Fadolalkarem, 2015).

Class	Relative impedance	Quadrant	*A*	*B*	Remarks
I	Higher than overlying unit	IV	+	−	Reflection coefficient (and magnitude) decrease with increasing offset
II	About the same as the overlying unit	III or IV	±	−	Reflection magnitude may increase or decrease with offset, and may reverse polarity
III	Lower than overlying unit	III	−	−	Reflection magnitude increases with offset
IV	Lower than overlying unit	II	−	+	Reflection magnitude decreases with offset

Table 5.3.1. This table explains the characteristics of each AVO class and how to identify which class the AVO response is (Castagna et al., 1998).

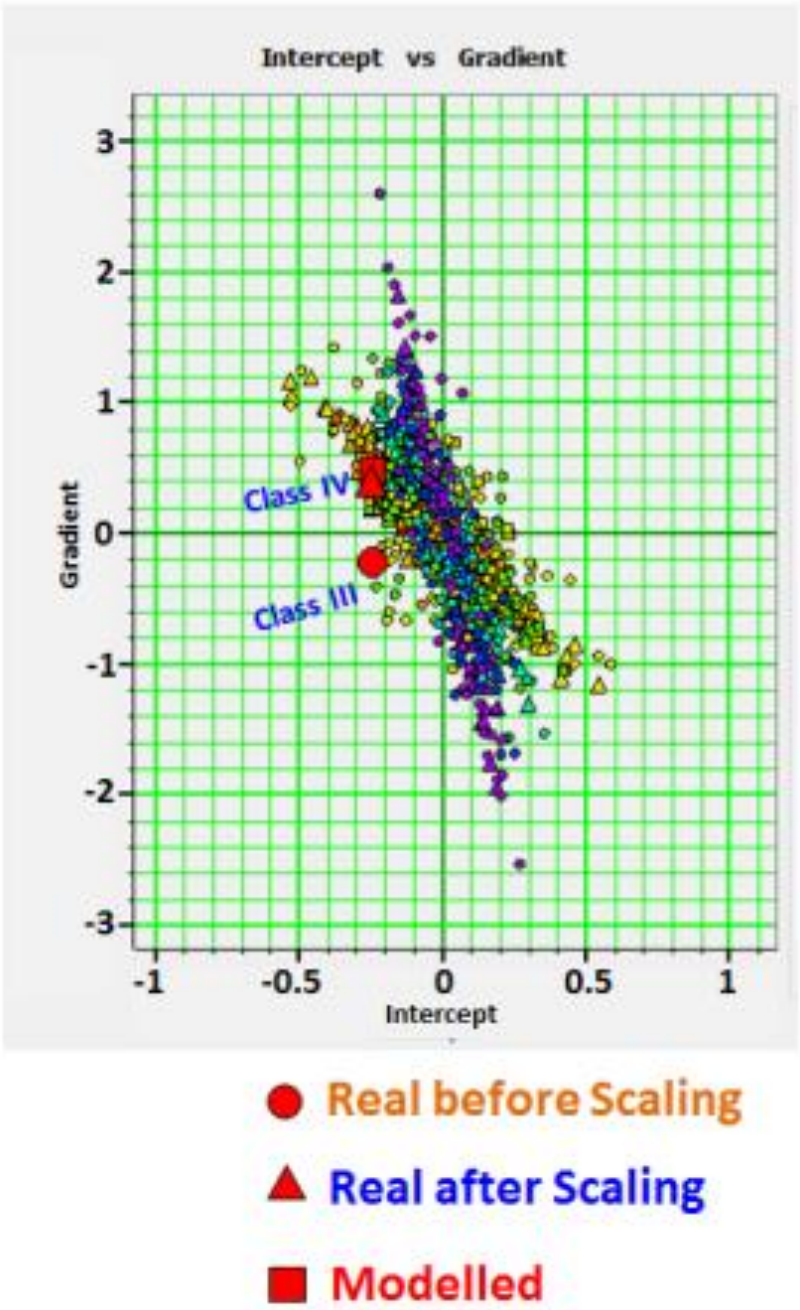

Figure 5.1.2. Intercept (A) – Gradient (B) crossplot from Fadolalkarem (2015) showing the location of the AVO response at KGS #1-32 for the actual seismic gathers before and after further processing, and the AVO response for the synthetic seismic gathers. The analysis indicates a Class IV AVO anomaly at the Mississippian reservoir; however, their data was reverse polarity, therefore it is more likely a Class I AVO response.

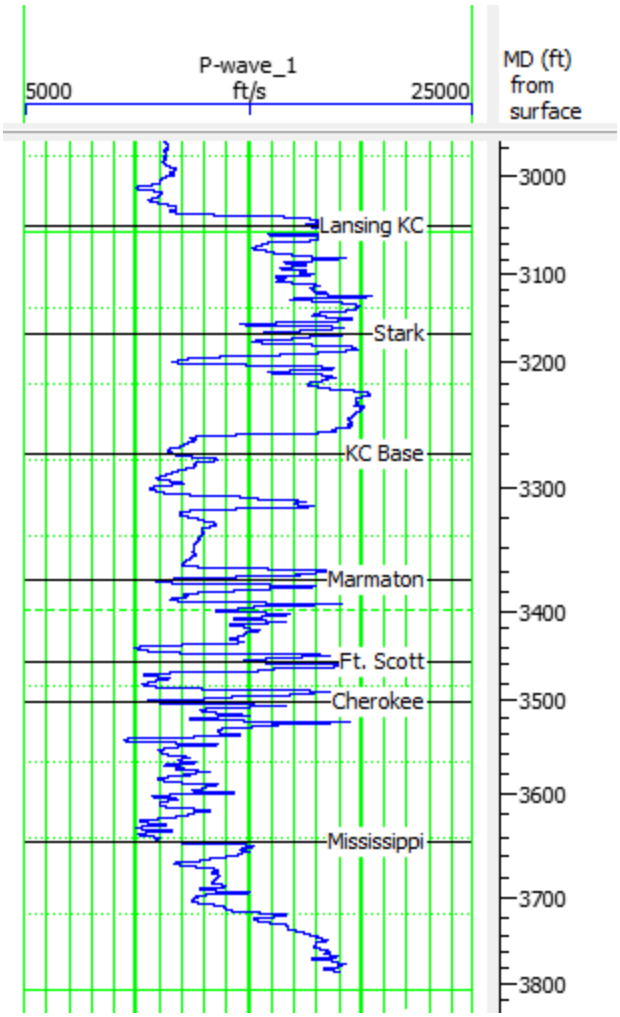

Figure 5.2.1. P-wave curve for KGS #2-32 used to generate the velocity log for AVO analysis. Log curves are from kgs.ku.edu and imported to Hampson-Russell Software.

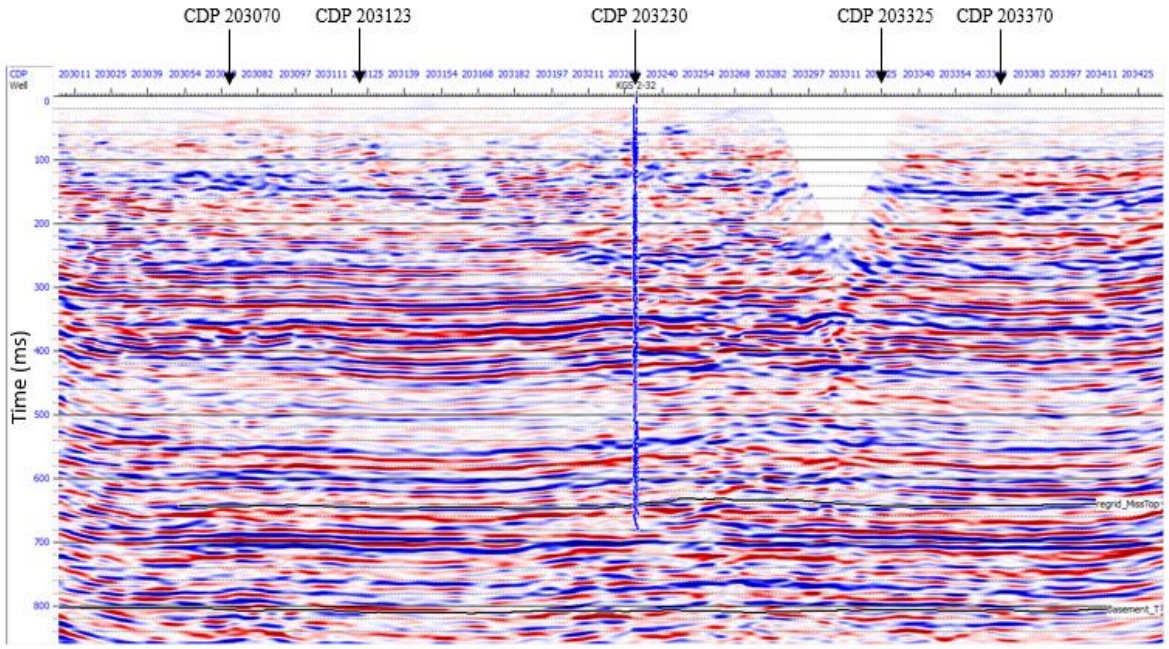

Figure 5.2.2. The location, on the 2-D post-injection post-stack seismic line, of the five CDP's used for AVO analysis. I compared the gradient curves for two CDP's from each side of the injection well to KGS 2-32 to identify changes in the curve. Generated in Hampson-Russell Software.

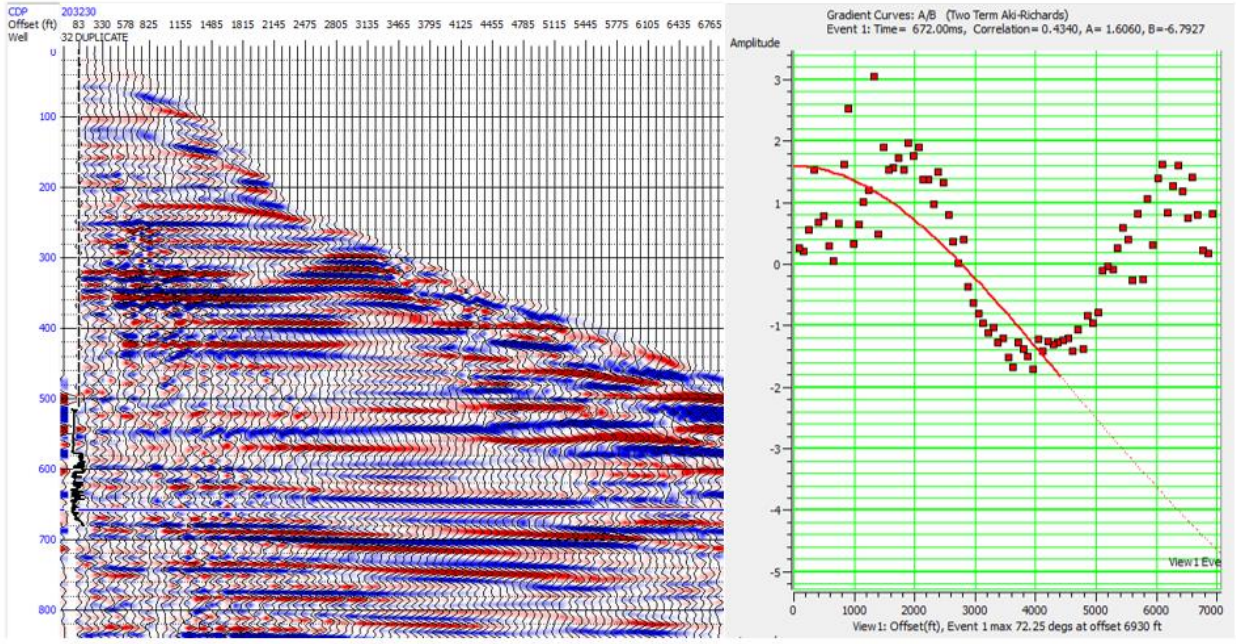

Figure 5.2.3. The seismic gathers (left) and gradient curve (right) for CDP 203230 (location of the injection well). The gradient curve is displayed in the offset domain up to 7,000 feet (2,133.5 meters). The AVO data is in general agreement to the modeled curve to approximately 4,000 feet or 1,219 meters. The theoretical modeled AVO curve is shown by the red line and red points.

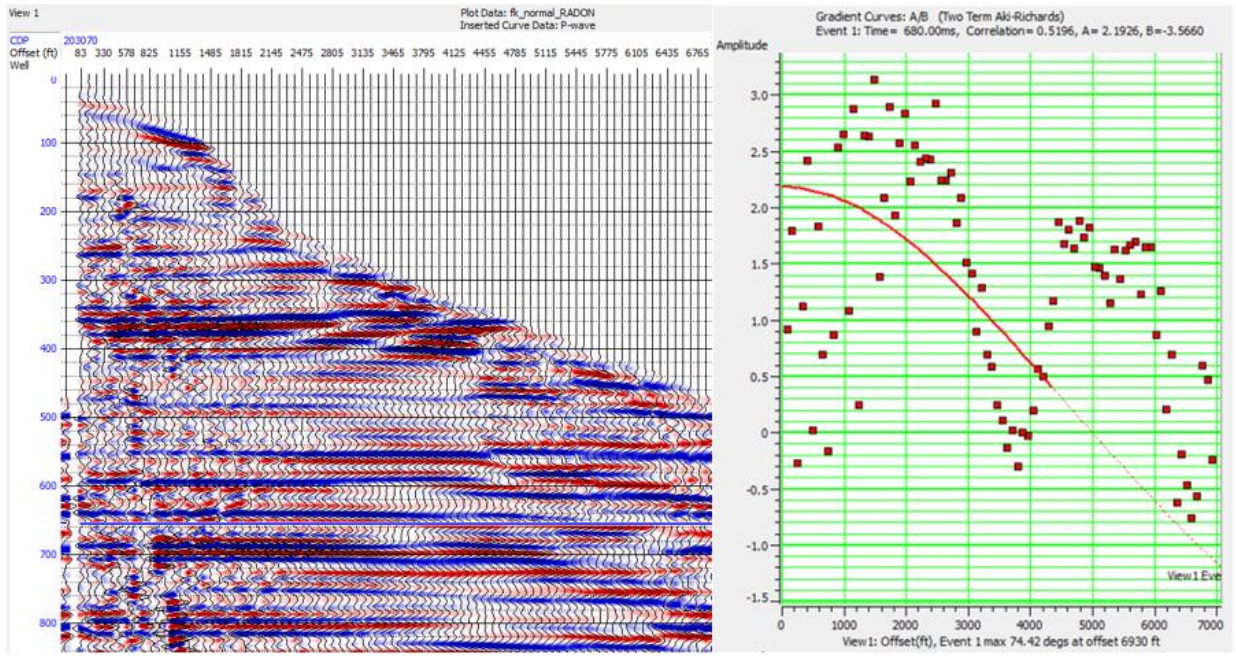

Figure 5.2.4. The seismic gathers (left) and gradient curve (right) for CDP 203070. CDP 203070 was one of two CDP's analyzed to the left of the injection well. The gradient curve displays a negative slope at the Mississippian reservoir, as well as, a decrease in amplitude with increasing offset. The theoretical modeled AVO curve is shown by the red line and red points.

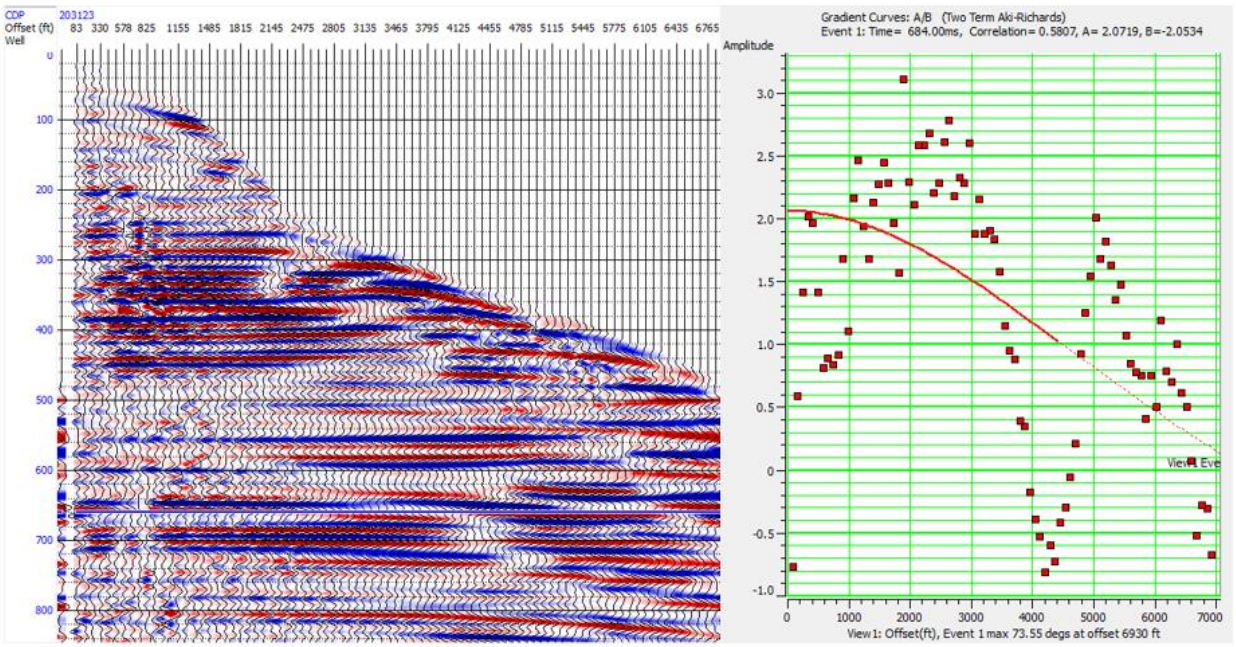

Figure 5.2.5. The seismic gathers (left) and gradient curve (right) for CDP 203123. This CDP is located on the left of the injection well and between CDP's 203070 and 203230. The gradient curve displays a similar trend as the gradient curve for CDP 203070. The theoretical modeled AVO curve is shown by the red line and red points.

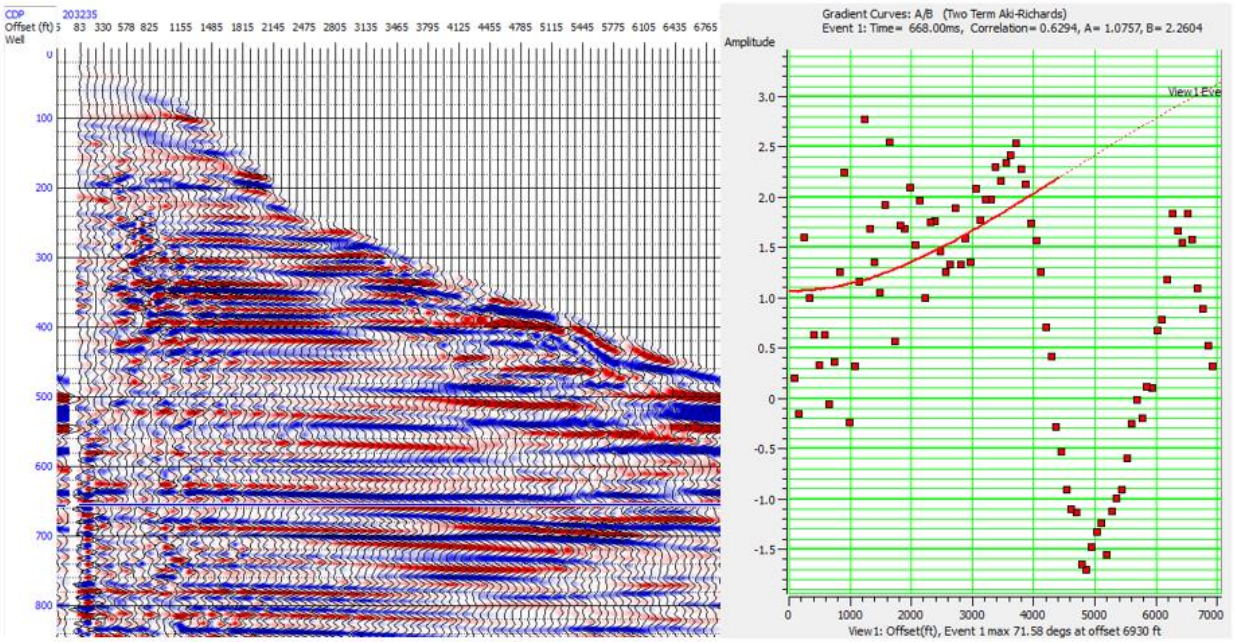

Figure 5.2.6. The seismic gathers (left) and gradient curve (right) for CDP 203325 at the Mississippian reservoir. The gradient curve is displayed in the offset domain up to 7,000 feet (2,133.5 meters) offset. The AVO data is in general agreement to the modeled curve to approximately 4,000 feet or 1,219 meters. The gradient curve exhibits a positive slope with increasing amplitude with offset up to approximately 4,000 feet offset, then the amplitudes decrease. The theoretical modeled AVO curve is shown by the red line and red points. This figure was generated in Hampson-Russell Software's Geoview module with AVO Analysis.

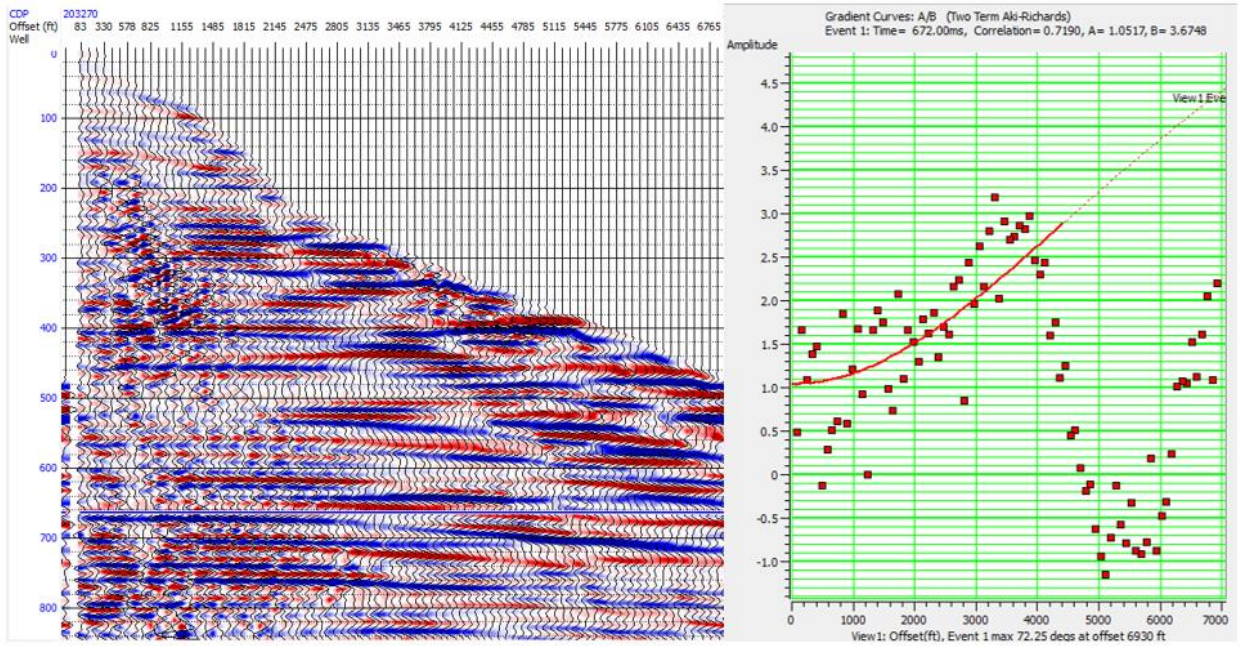

Figure 5.2.7. The seismic gathers (left) and gradient curve (right) for CDP 203370 at the Mississippian reservoir but to the right of the injection well. The gradient curve exhibits a similar trend as CDP 203325 (figure 5.2.6). The theoretical modeled AVO curve is shown by the red line and red points.

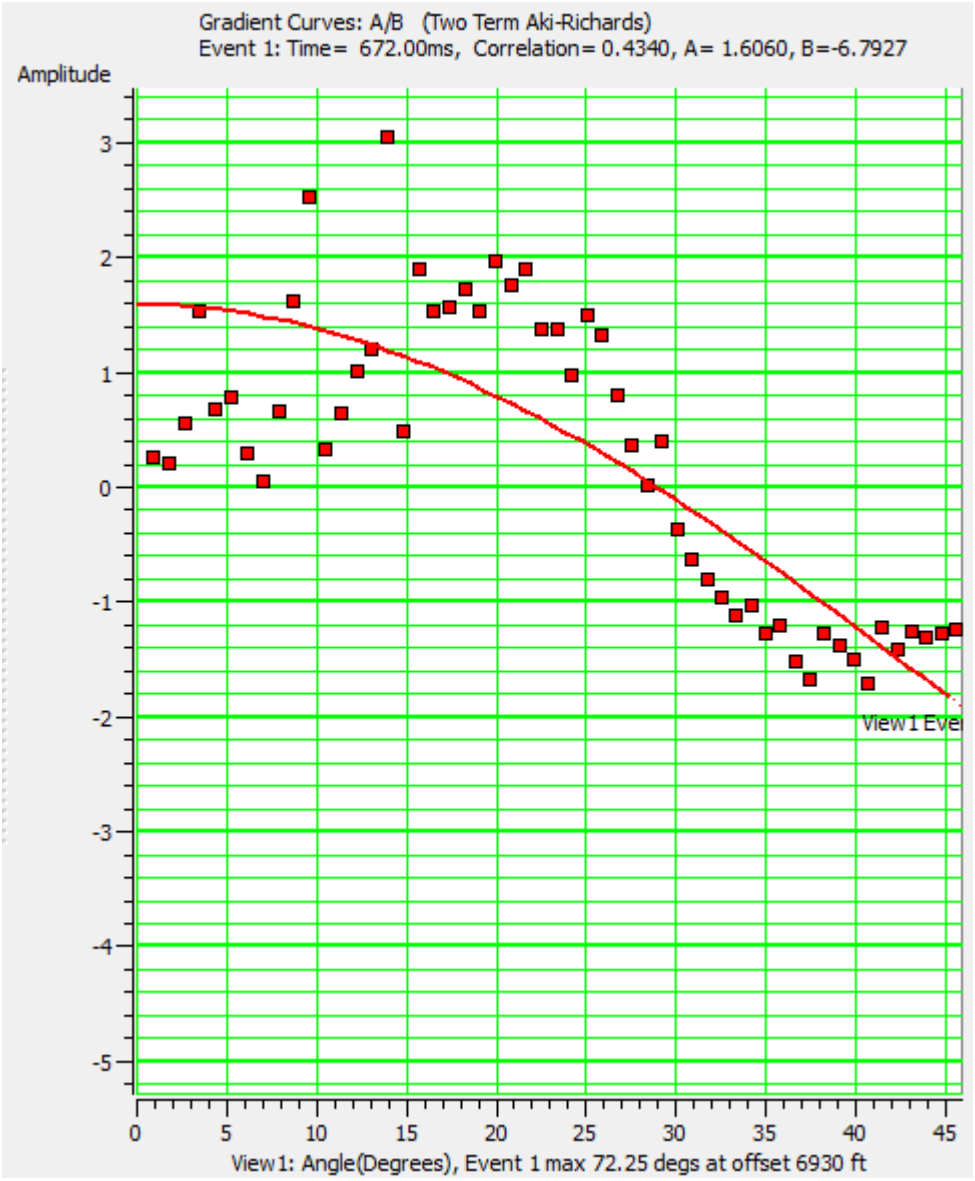

Figure 5.2.8. The AVO gradient curve for CDP 203230 (location of KGS #2-32) at the Mississippian reservoir in the angle domain. The sinusoidal shape is present. This figure was generated in Hampson-Russell Software.

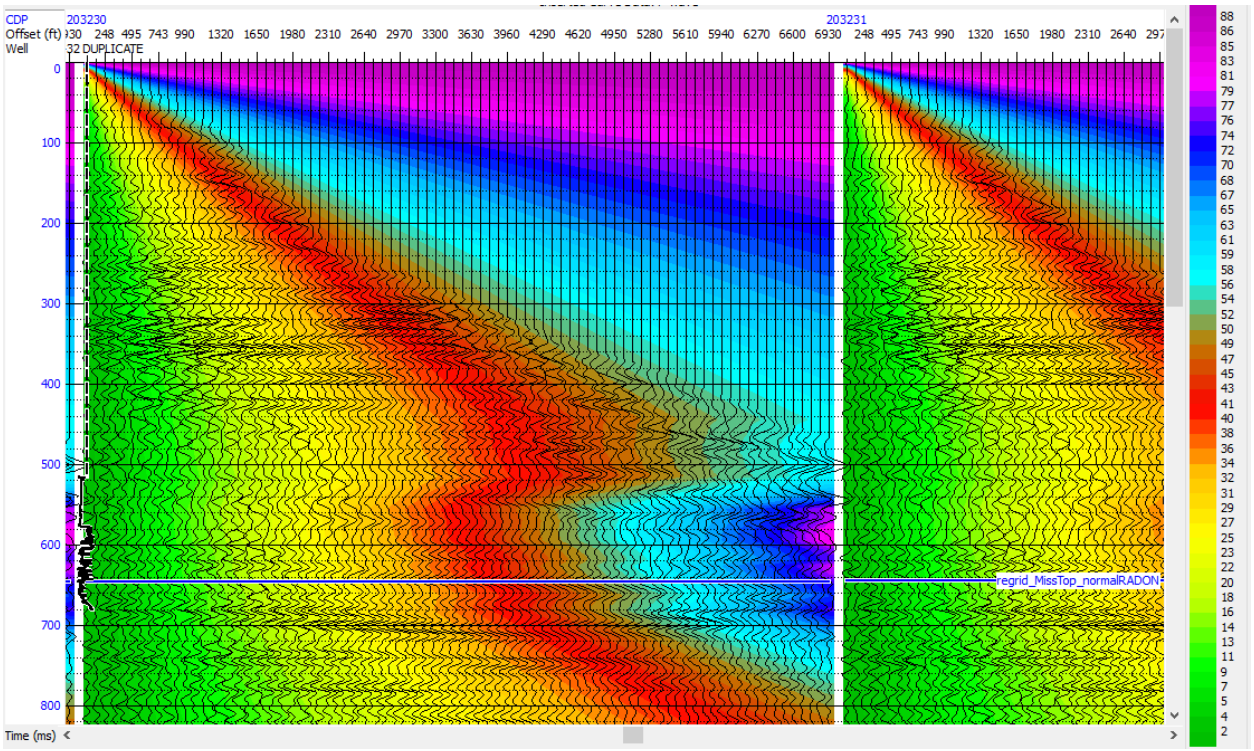

Figure 5.2.9. The angle of incidence for the 2-D post-injection seismic gathers at KGS #2-32. Generated in Hampson-Russell Software.

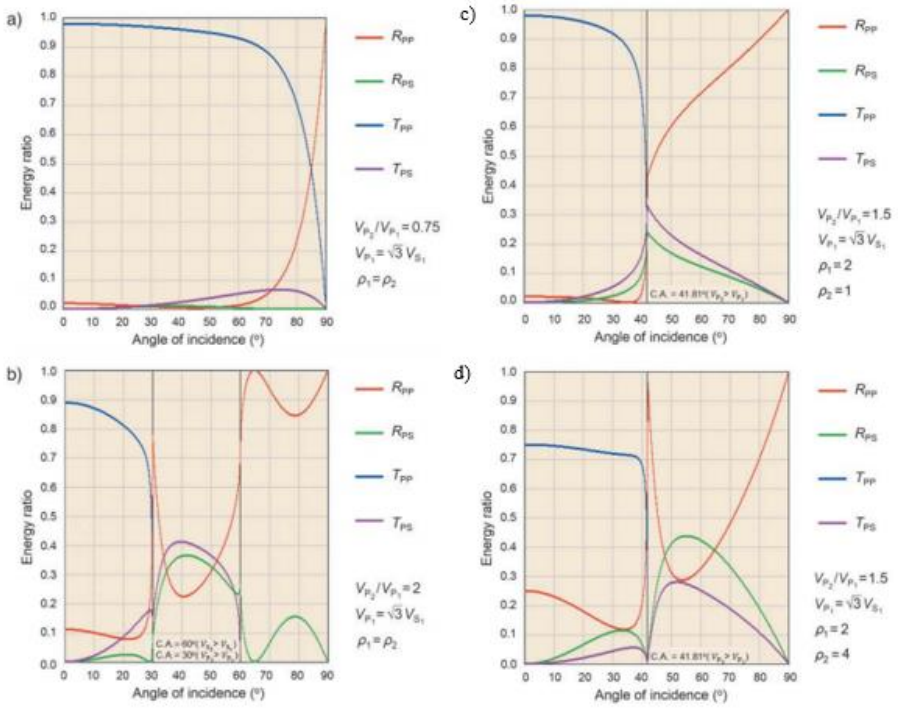

Figure 5.2.10. Zoeppritz equations are mathematical statements of the boundary conditions in energy partitioning at an interface. As shown above, there are multiple different scenarios depending on the values for p-wave velocity, s-wave velocity, and density; however, the critical angle is from 30-45 degrees for each scenario. These curves display the effects of approaching the critical angle and also why we should expect a sinusoidal shape around 30-40 degrees in our AVO analysis (Chopra and Castagna, 2014).

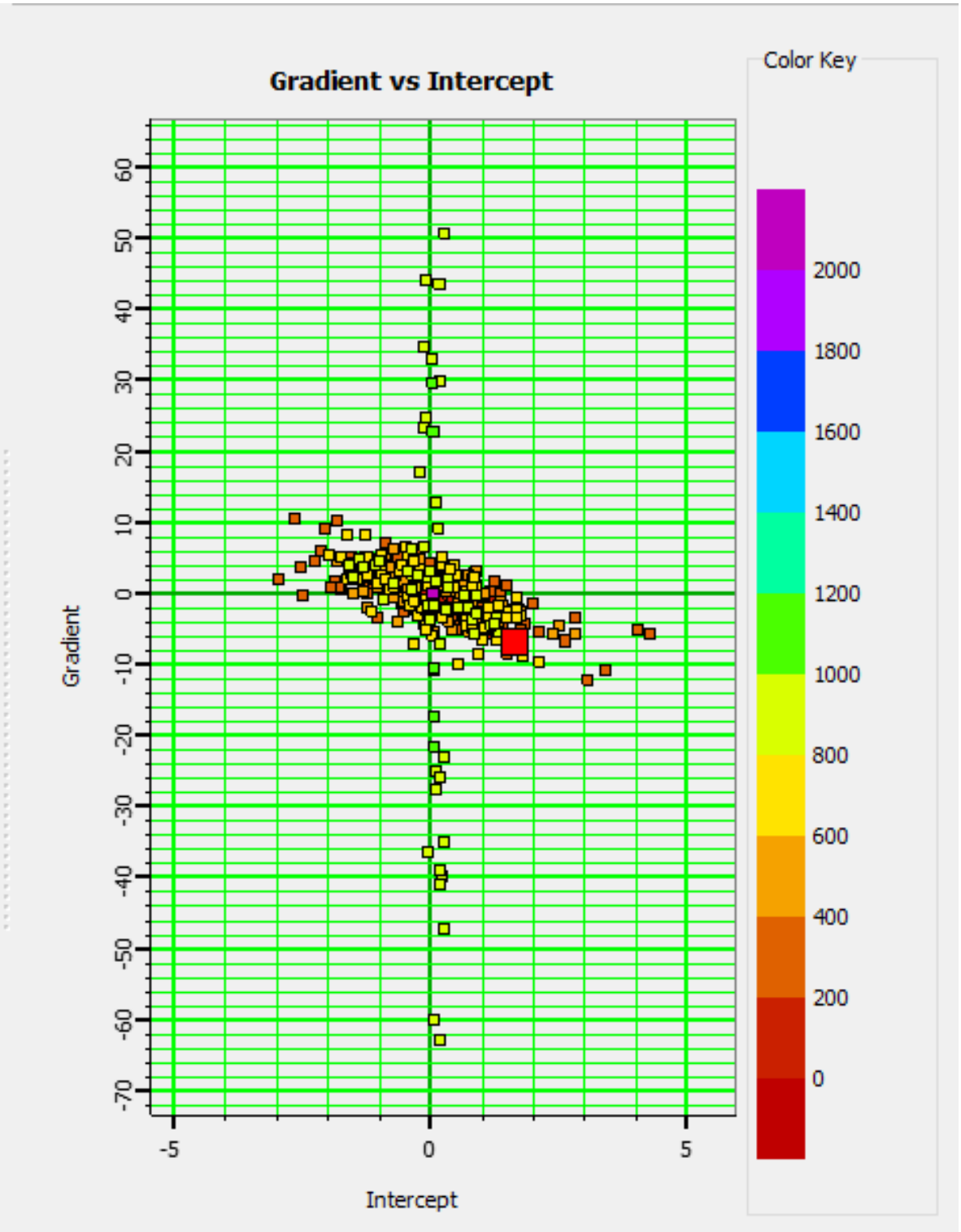

Figure 5.2.11. The A-B crossplot for CDP 203230 on the 2-D post-injection seismic line with f-k filtering applied. Generated in Hampson-Russell Software. The large red square is the location of the Mississippian reflector AVO response.

CHAPTER 6: DISCUSSION AND CONCLUSIONS

Section 6.1 Discussion

Utilizing multiple seismic analysis methods to image a CO_2 injection is a common method used in many case studies throughout the world and shown to be successful (Ivanova et al., 2013). These techniques include time-lapse seismic analysis, fluid substitution modeling, and amplitude variation with offset (AVO) analysis. Each of these techniques were applied to a seismic dataset acquired in Wellington field, Sumner County, Kansas, and analyzed to see if we could image the CO_2 injection in the Mississippian reservoir using seismic data. Seismic data analysis is integrated with well control for a more accurate interpretation of the subsurface around the injection well.

The use of time-lapse seismic analysis to image a CO_2 injection has been applied in many case studies throughout the world. In this study, one post-injection 2-D seismic line was acquired and directly crossed through the injection well; however, it did not overlay any of the pre-injection 2-D seismic lines for a direct time-lapse comparison. An arbitrary line extracted from the pre-injection 3-D seismic survey was used for time-lapse analysis with the post-injection 2-D seismic line. While time-lapse seismic analysis has been successful for monitoring CO_2 injections in other studies, it is highly dependent upon multiple factors. Some of the factors include unit thickness, data quality, local geology, and amount of CO_2 injected. Since our analysis focused on the comparison of a 2-D seismic line versus an arbitrary line extracted from 3-D seismic data, we were primarily able to see the differences in data quality between 2-D and 3-D datasets. Reflectors in the 2-D seismic data were a lot less continuous throughout the entire seismic section than the 3-D dataset. In addition, the arbitrary line from the 3-D dataset exhibited strong reflectors in areas where reflectors were not highly visible in the 2-D seismic

data. Each of these observations was not unexpected due to the known differences in data quality between 2-D and 3-D datasets. There was also a relatively small amount of CO_2 injected at the Mississippian reservoir which makes it challenging to use time-lapse seismic analysis to monitor it. Previous case studies have proven time-lapse seismic analysis to be effective in imaging CO_2 in the subsurface; however, the majority of these studies injected more CO_2 than our study and acquired the proper seismic data pre- and post-injection. Our next approach focused on another common seismic analysis method: fluid substitution modeling.

Fluid substitution modeling is commonly utilized to model various possible fluid scenarios at an injection point to determine how the introduction of a fluid affects seismic properties, such as impedance. Previous work by Graham et al. (2016) modeled the effects of CO_2 in the Mississippian reservoir around the injection site using arbitrary fluid parameters to test the effectiveness of the method. Graham et al. (2016) created models using both Gassmann and Patchy fluid substitution models with only water and CO_2 taken into account. Ultimately, their study concluded that there could be up to a 10% decrease (larger absolute value) in normal incidence impedance in the Mississippian reservoir due to the introduction of CO_2. This observation was confirmed in our study using actual subsurface values obtained post-injection by Eugene Holubnyak (personal communication, 2017). In addition to CO_2 and water saturations, our study took oil saturations into account as well. Similar to Graham et al. (2016), this study focused on analyzing both Gassmann and Patchy fluid substitution modeling to determine the best fit for our dataset. Patchy modeling was primarily used because it provides a higher accuracy for saturations greater than 20% and the CO_2 saturation around the injection well is as high as 50% in some areas. In this study, these models displayed a decreasing (larger absolute

value) normal incidence impedance with increasing CO_2 saturation; this is an expected result for CO_2 fluid substitution modeling.

Amplitude variation with offset (AVO) is extremely sensitive to noise and processing artifacts, therefore, further processing of the 2-D post-injection seismic gathers was required for more accurate AVO analysis. Low-frequency coherent linear noise was identified in the seismic gathers, so a f-k filter was created and applied to the data to remove the noise. The f-k filter was successful in removing the noise and improving the A-B crossplot. Next, trim statics was applied to correct for residual normal move-out (RNMO) errors which distort the estimation of the gradient. Multiple trim statics analysis windows were applied to the data; however, results were inconclusive, and the reflectors did not flatten as expected. The final processing step applied to this data was AVO Offset Scaling to correct for processing artifacts introduced by previous processing steps. Similar to trim statics, AVO Offset Scaling was inconclusive with our dataset and did not help improve the A-B crossplots as expected. Overall, the f-k filter was the most effective processing step applied to remove linear coherent noise and improve the A-B crossplot for AVO analysis.

Amplitude variation with offset was used to analyze the standard AVO attributes, intercept (A) and gradient (B), at the Mississippian reservoir post-injection near and far from the injection site. This was to identify any possible discrepancies in the seismic data to determine if they were caused by the introduction of CO_2. Both gradient curves and A-B crossplots were analyzed at multiple locations throughout the entire length of the seismic line. Gradient curves presented a sinusoidal shape throughout the majority of CDP's along the seismic line, specifically CDP 203230 (site of the injection well). I analyzed CDP's along the seismic line in increments of 5 to try to identify any changes in the gradient curve near and far from the

injection well; however, the majority of the CDP's throughout the entire seismic line exhibited the same sinusoidal shape or were extremely scattered. Based on the Zoeppritz equations describing partition of energy at an interface, the sinusoidal shape can be attributed to approaching the critical angle. The A-B crossplots were then analyzed for multiple CDP's near and distant from the injection site. At KGS #2-32, the Mississippian reflector was plotted in quadrant IV which is indicative of a Class I AVO anomaly. Overall, the crossplots and curves were too scattered to be reliable enough to determine changes in CO_2 saturation throughout the Mississippian reservoir, although CDP 203230 behaves better than the CDP's away from the well on either side of the seismic line.

These processing steps and AVO analysis have been successfully applied to this dataset before with a focus on the Mississippian reservoir by Fadolalkarem (2015); however, their work focused on the 3-D pre-injection seismic data before it was re-processed by FairfieldNodal. Each of these seismic analysis methods have also been analyzed in multiple case studies around the world and have been successful in imaging a CO_2 injection. Although most of these studies injected a larger amount of CO_2 than our study, therefore, making it easier to image. Some other challenges we ran into included that the zone of interest (Mississippian reservoir) is composed of carbonates and its thickness is below seismic resolution which makes it challenging to detect changes in pore fluids. In addition, near surface conditions were poor during acquisition of the post-injection 2-D line due to heavy rain making the ground soft and resulting in interruption of field acquisition operations. Another challenge I faced was the re-processing of the data which made it noisier, although it did preserve a more accurate relative amplitude. Except for the success of fluid substitution modeling, these challenges made it difficult to truly image the CO_2 injection in the Mississippian reservoir.

Section 6.2: Conclusions

From January to June 2016, the Kansas Geological Survey injected approximately 20,000 metric tons of CO_2 into the Mississippian reservoir at Wellington field for enhanced oil recovery and geologic storage. Some challenges that needed to be taken into account in this study include the relatively small amount of CO_2 injected, the high matrix incompressibility of a carbonate, and spatial heterogeneity of material properties. The CO_2 volume challenge was specific to this study; however, the incompressibility and heterogeneity issues are more general challenges when imaging CO_2 in carbonate rocks.

Multiple seismic analysis methods were employed to analyze and interpret the subsurface post-injection to identify discrepancies in the data possibly introduced by the CO_2 injection. Initially, the 3-D pre-injection seismic survey and 2-D post-injection seismic line were utilized for time-lapse seismic analysis; however, this was inconclusive due to the difference in data quality. Fluid substitution modeling suggested a normal incidence impedance decrease (larger absolute value) of up to 6.1% with 25% CO_2 saturation, the average saturation around the injection site. The models also show a continually decreasing impedance with increasing CO_2 saturations.

Secondly, AVO analysis was performed on the post-injection seismic gathers. Before amplitude variation with offset analysis was completed, further processing was applied to the seismic gathers. Since AVO is extremely sensitive to noise, three processing steps including f-k filtering, trim statics, and AVO Offset Scaling (Appendix A-C) were applied to this dataset to remove linear coherent noise and improve the A-B crossplot. Amplitude variation with offset analysis concluded that the reservoir reflector displays a Class I AVO anomaly. While the crossplot and gradient curves were scattered, we were able to identify a trend throughout the

curves. The CDP at the injection well displayed less scatter than the CDP's on either side, as well as, the CDP's to the left and right followed their own trends, respectively. Both fluid substitution modeling and AVO analysis presented in this study offer insights to the effectiveness of methods, as well as shortcomings, their sources and how to overcome them, which will be valuable in future investigation of seismic imaging of CO_2 injected in carbonate reservoirs in Kansas.

APPENDIX

Appendix A: F-K Filtering

Through further analysis of the 2-D post-injection seismic gathers, we noticed there was a low-frequency coherent linear noise in the data (Figure A-1). This kind of noise significantly affects Amplitude Variation with Offset analysis, specifically the AVO crossplot. The crossplot becomes more scattered, therefore it is less reliable. Coherent linear noise can be separated from the reflection energy in the f-k domain through F-K filtering. An F-K filter was applied to the seismic gathers to remove the noise and improve the AVO crossplot. The primary steps of F-K filtering, according to Yilmaz (1987), are shown in Figure A-2. I applied three F-K filters of differing severities (conservative, moderate, and severe) to determine the best filter for the dataset. The F-K filter works by isolating the low-frequency coherent noise from the reflection energy in the (f, k) space. First, a 2-D Fourier transform is applied to the seismic gathers to transform them from the (t, x) space to the (f, k) space (Figure A-3). The seismic gathers were cut at 900 ms to remove some of the noise in the (f, k) space but to include the Arbuckle reservoir and some of the basement. Once the seismic gathers are in the f-k domain a fan reject zone is defined to remove the low-frequency coherent noise from the input dataset (Figure A-4a-4c) (Yilmaz, 1987). Then, the data is transformed back to the (t, x) space by applying the 2-D inverse Fourier transform to the filtered dataset (Figure A-5a-5c). The normal F-K filter removed the low-frequency coherent linear noise without removing actual data (Figure A-6). The filter also improved the correlation of the AVO crossplot and made it less scattered. Although the majority of my seismic interpretation and analysis was completed in Hampson-Russell Software, the F-K filter was created and applied to the input dataset in Schlumberger's VISTA Seismic Processing Software. The filtered dataset is exported in SEG-Y format from

VISTA to Hampson-Russell Software to enhance further pre-stack seismic interpretation and analysis, including AVO analysis.

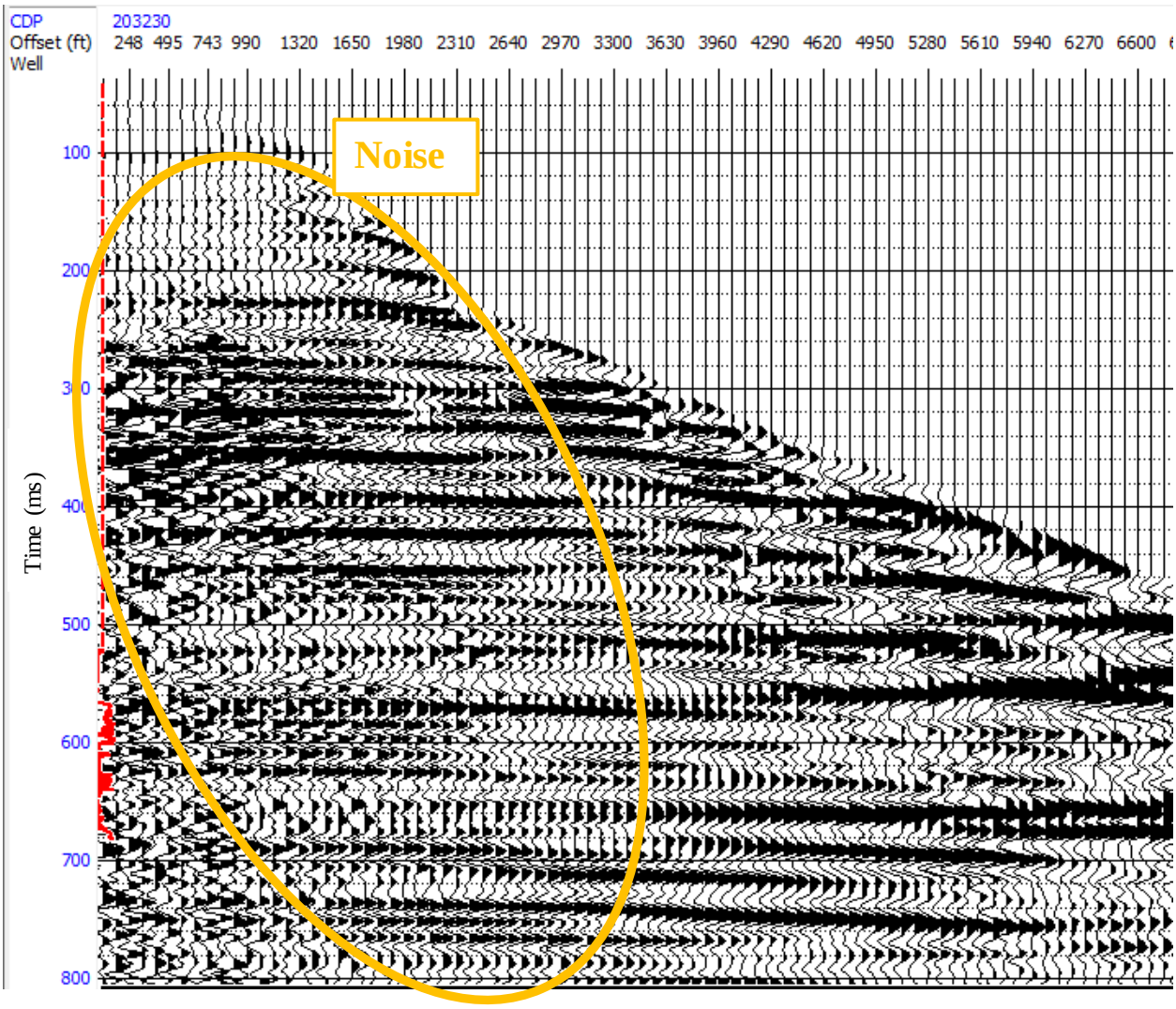

Figure A-7. PSTM seismic gathers from seismic line 03 at CDP 203230, the location of KGS #2-32. The figure shows the low-frequency coherent noise in the data. Figure was generated in Hampson-Russell Software.

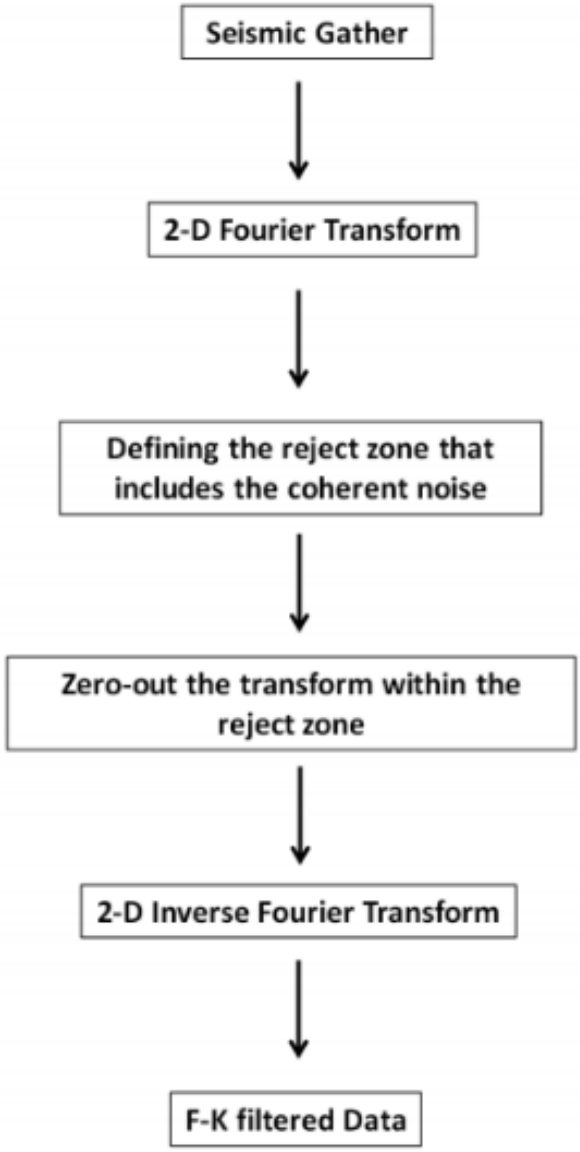

Figure A-8. Flow chart of the F-K filter process. (Yilmaz, 1987).

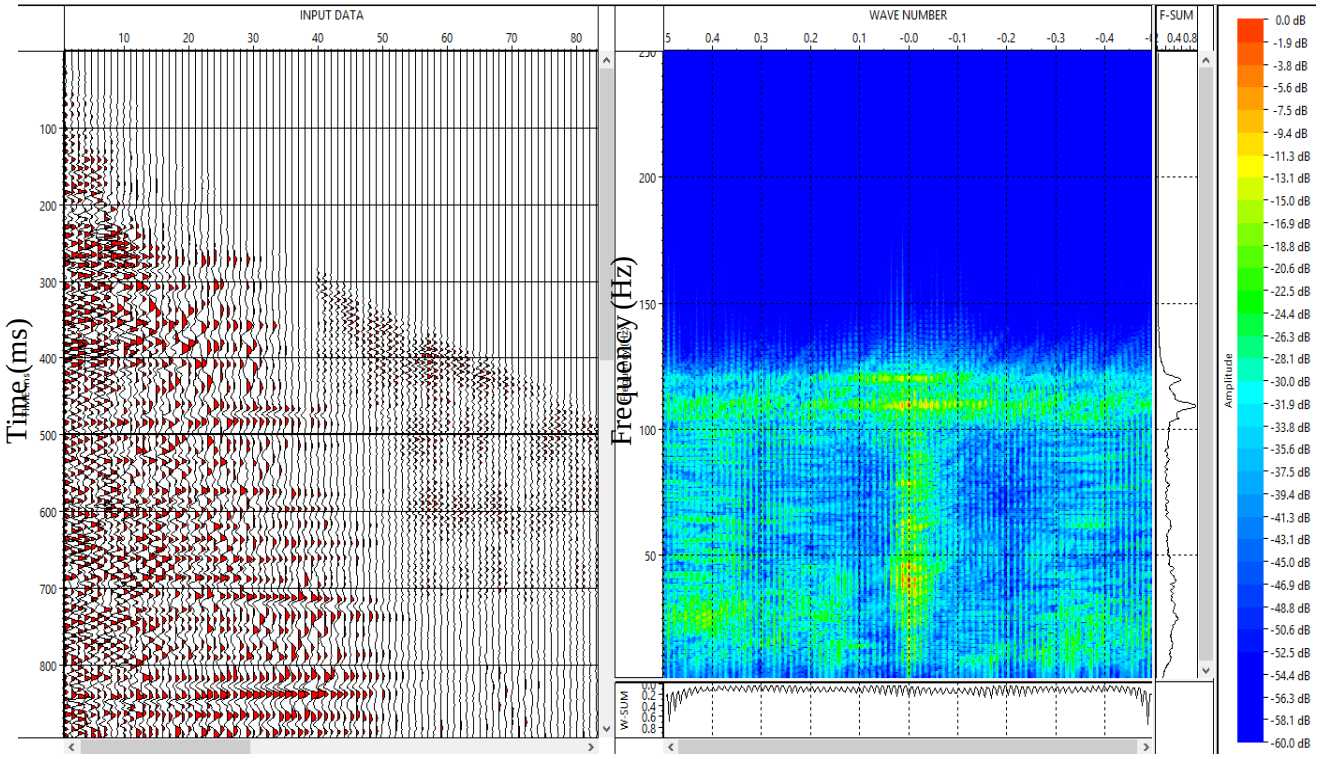

Figure A-3. The first step in the f-k filter process is to transform the seismic data from the time domain (left) to the (f, k) space (right). This was done using VISTA Seismic Processing Software.

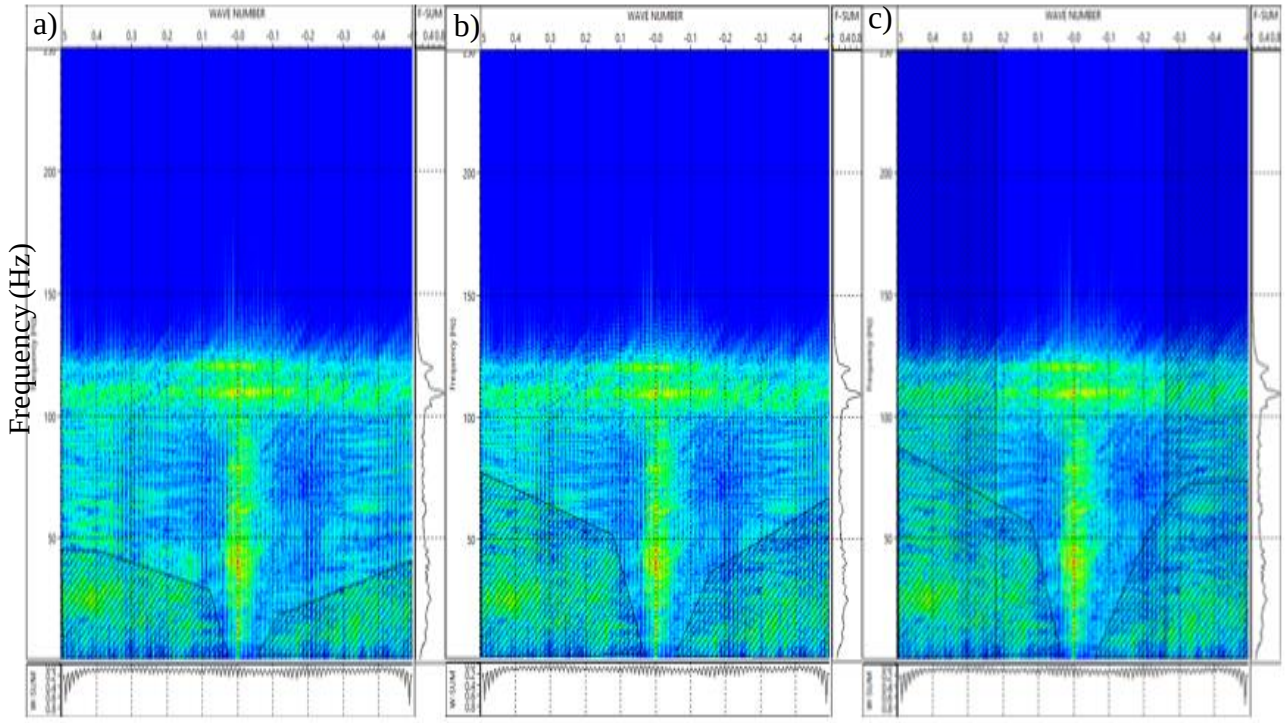

Figure A-4a-c. The f-k rejection zone is defined for the three different severities of f-k filters applied to this data. The x-axis is the wave number and the y-axis is frequency in Hertz. The conservative rejection zone is in (a). The normal rejection zone is in (b). The severe rejection zone is shown in (c). F-k filtering was completed using VISTA Seismic Processing Software.

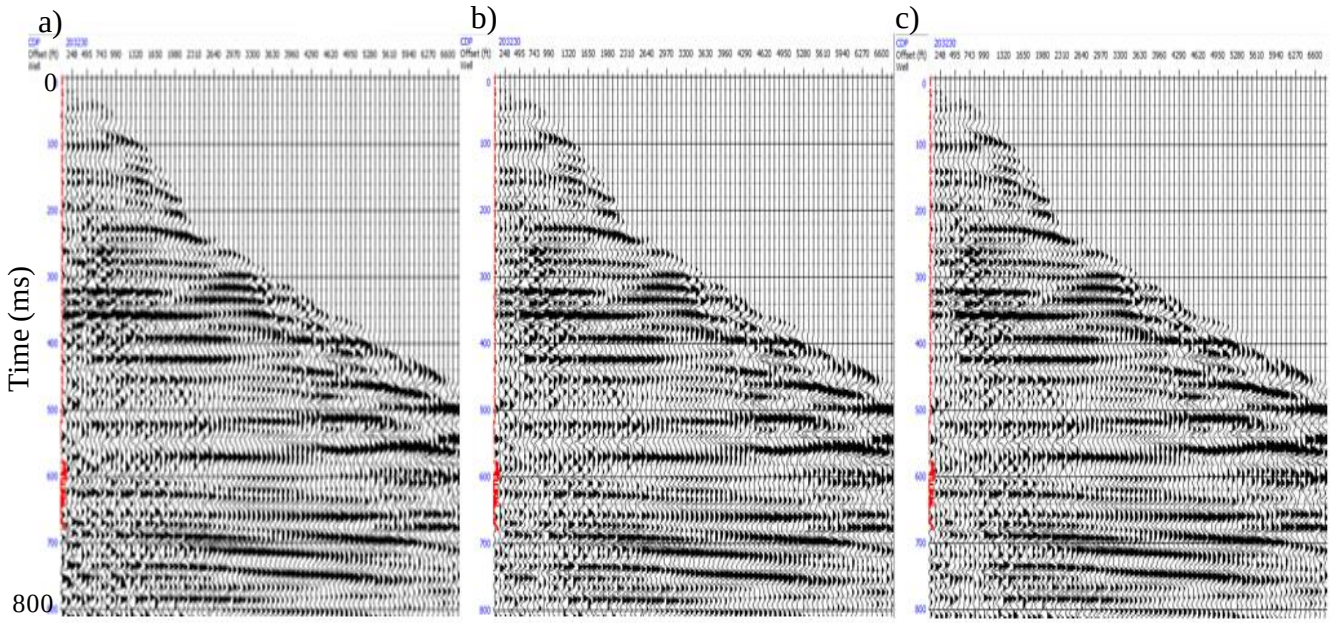

Figure A-5a-c. The filtered seismic gathers at the location of KGS #2-32 (CDP 203230). a) The seismic gathers with the conservative f-k filter applied. b) The seismic gathers with the normal f-k filter applied are displayed. c) The seismic gathers with the severe f-k filter applied are shown. The y-axis is in time (ms) with the Mississippian reservoir around 640ms. These figures were generated in Hampson-Russell Software.

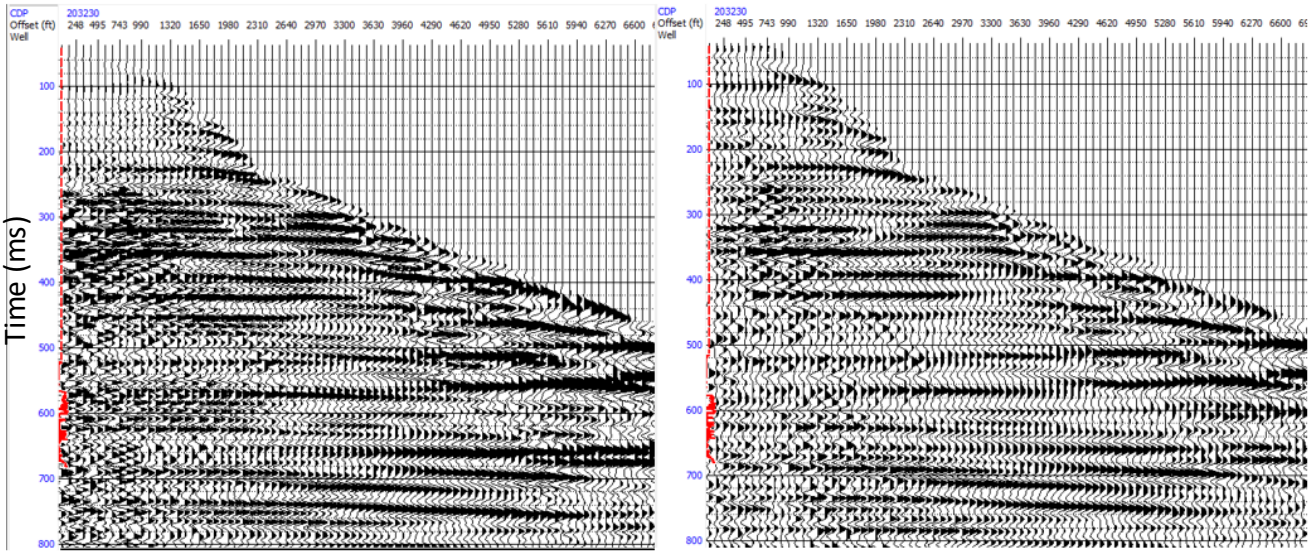

Figure A-6. Comparison of the original seismic gathers with coherent linear noise (left) and the normal f-k filtered data (right). These seismic gathers are at the location of the injection well, KGS #2-32 (CDP 203230). In the pre-filter data, there is a lot more noise and the reflectors are a lot less clear.

Appendix B: Trim Statics

Trim statics is the process of correcting for RNMO (residual normal move-out) errors on pre-stack seismic gathers. RNMO errors distort the estimation of the gradient and any other related attributes (Figure B-1; Ratcliffe and Roberts, 2003). Trim statics processing is able to be completed using Hampson-Russell Software. The input parameters for trim statics include the seismic line, time window, CDP range, offset range, and the trim statics analysis window. I applied trim statics to the 2-D post-injection seismic line (with f-k filtering applied) with a time window from 0 to 900 milliseconds. All parameters stayed the same for each trial except the trim statics analysis window. This window was also centered on the Mississippian reservoir reflector. The window value varied from 150 to 300 milliseconds. Multiple trim statics analysis windows were utilized to find the best fit for this dataset. Trim statics processing begins with creating a pilot trace, which is typically the stacked trace of each gather. Next, each trace is correlated with the pilot trace and the cross correlation is used to calculate the optimal time shift. Finally, all time shifts are interpolated to generate a time-variant stretch of the trace, which typically results in aligned events (Fadolalkarem, 2015). Trim statics analysis windows of 150 milliseconds (Figure B-2) and 300 milliseconds (Figure B-3) were both applied to the post-injection 2-D pre-stack seismic gathers and analyzed; however, neither window flattened reflectors in the zone of interest as expected.

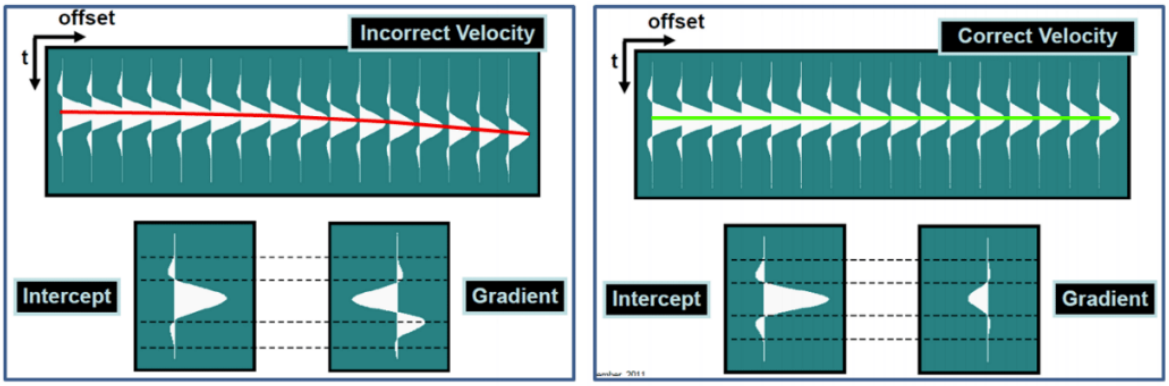

(a) (b)

Figure B-9. a) A reflection event with residual normal move-out (RNMO) error. b) The reflection event with the correct velocity resulting in a flattened reflector. Notice the difference in the intercept and gradient for both figures due to the RNMO errors. Modified from Ratcliffe and Roberts (2003).

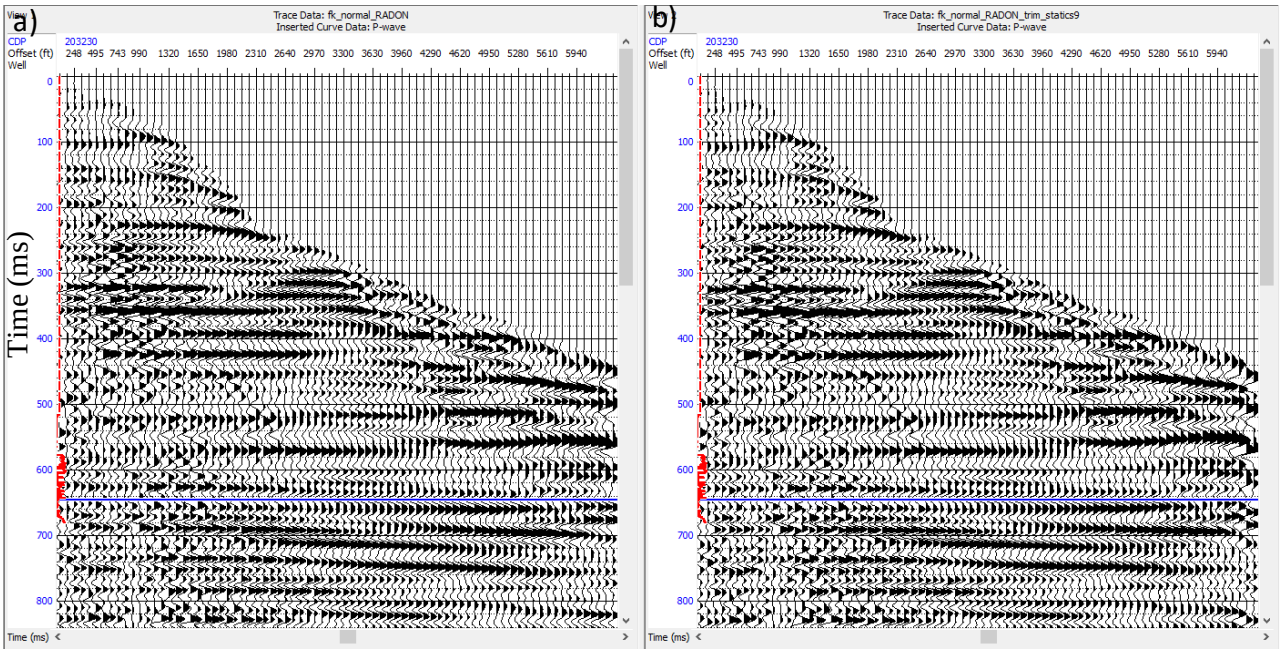

Figure B-2. a) The seismic gather before trim statics was applied. b) The seismic gather after trim statics was applied with a 150 milliseconds trim statics analysis window. The top of the Mississippian horizon is outlined in blue and the location of KGS #2-32 is displayed in red. Generated in Hampson-Russell Software.

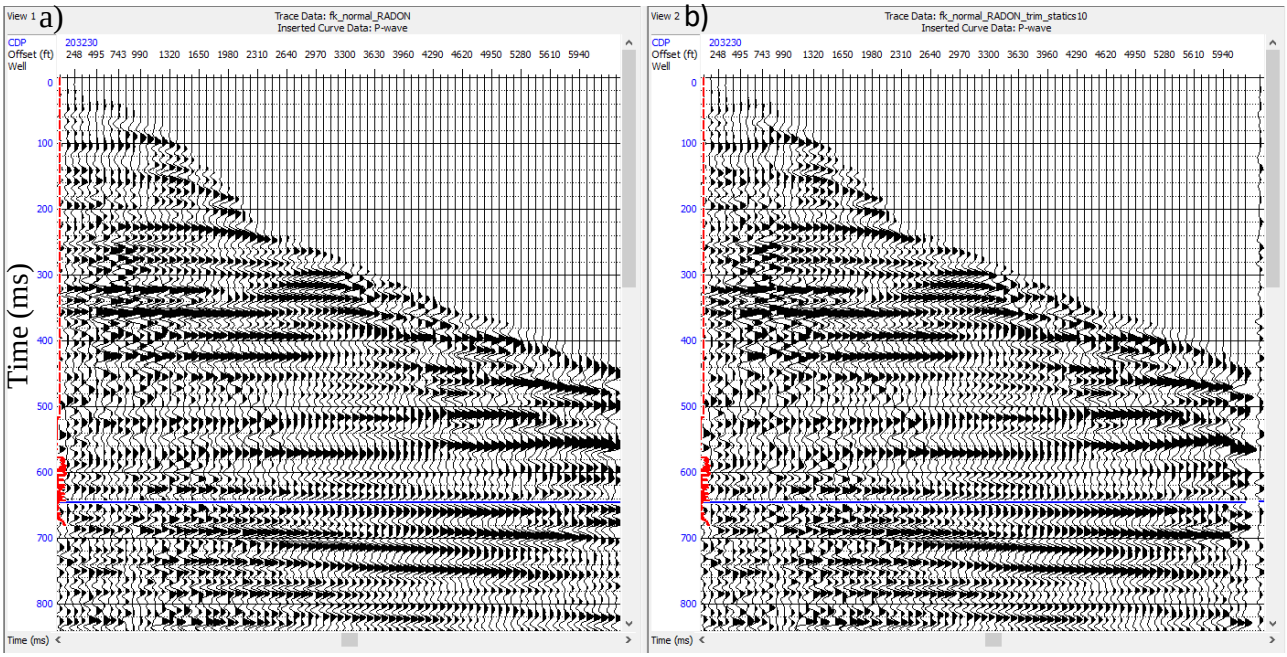

Figure B-3. a) The seismic gather before trim statics was applied. b) The seismic gather after trim statics was applied with a 300 milliseconds trim statics analysis window. The top of the Mississippian horizon is outlined in blue and the location of KGS #2-32 is displayed in red. Generated in Hampson-Russell Software.

Appendix C: AVO Offset Scaling

AVO Offset Scaling is a seismic processing technique in Hampson-Russell Software (HRS) and used to correct for a systematic offset-dependent amplitude distortion in pre-stack seismic gathers. It is also a data conditioning method utilized to correct for processing artifacts and distortions created by under-correction or overcorrection from previous processing. There are two main steps in AVO Offset Scaling in HRS: analysis and application. In AVO Offset Scaling Analysis the offset scaling value is defined for the test windows (Li and Worsick, 2012). AVO Offset Scaling Apply is then used to apply this offset scaling value to the zone of interest, which in our study is the Mississippian reservoir reflector.

Although there are two main steps in AVO Offset Scaling in HRS, each step has sub-steps. First, you create a pure brine synthetic to determine the standard AVO response and derive the background parameters for scaling. Once the pure brine synthetic is created, application and model volumes are created. The application volume uses the 2-D post-injection seismic line with f-k filtering applied, while the model volume uses the pure brine synthetic. During this process, the intercept and gradient are calculated for all real seismic gathers within a non-target zone. This zone is designed to be from 0 to 620 milliseconds to avoid any possible reservoir, which is the Mississippian beginning at 640 milliseconds in this study. In addition to avoiding potential reservoirs, it is also important to avoid areas of complex lithology, strong structures (i.e. faulting), and salt features (Li and Worsick, 2012). The intercept and gradient are calculated for the modeled volume over the same time window for the injection well, KGS #2-32. As shown in figure C-1, the mean gradient trend of the actual seismic data and the modeled seismic data show good agreement until approximately 4,000 feet (1,219 meters) in offset; however, they do not match well in the far offsets. Therefore, the offset-dependent scalars are

applied to the real seismic data to try to make the actual seismic gathers mean trend match the trend of the modeled volume (Fadolalkarem, 2015). Figure C-2 shows the actual seismic data before and after the AVO Offset Scaling was applied.

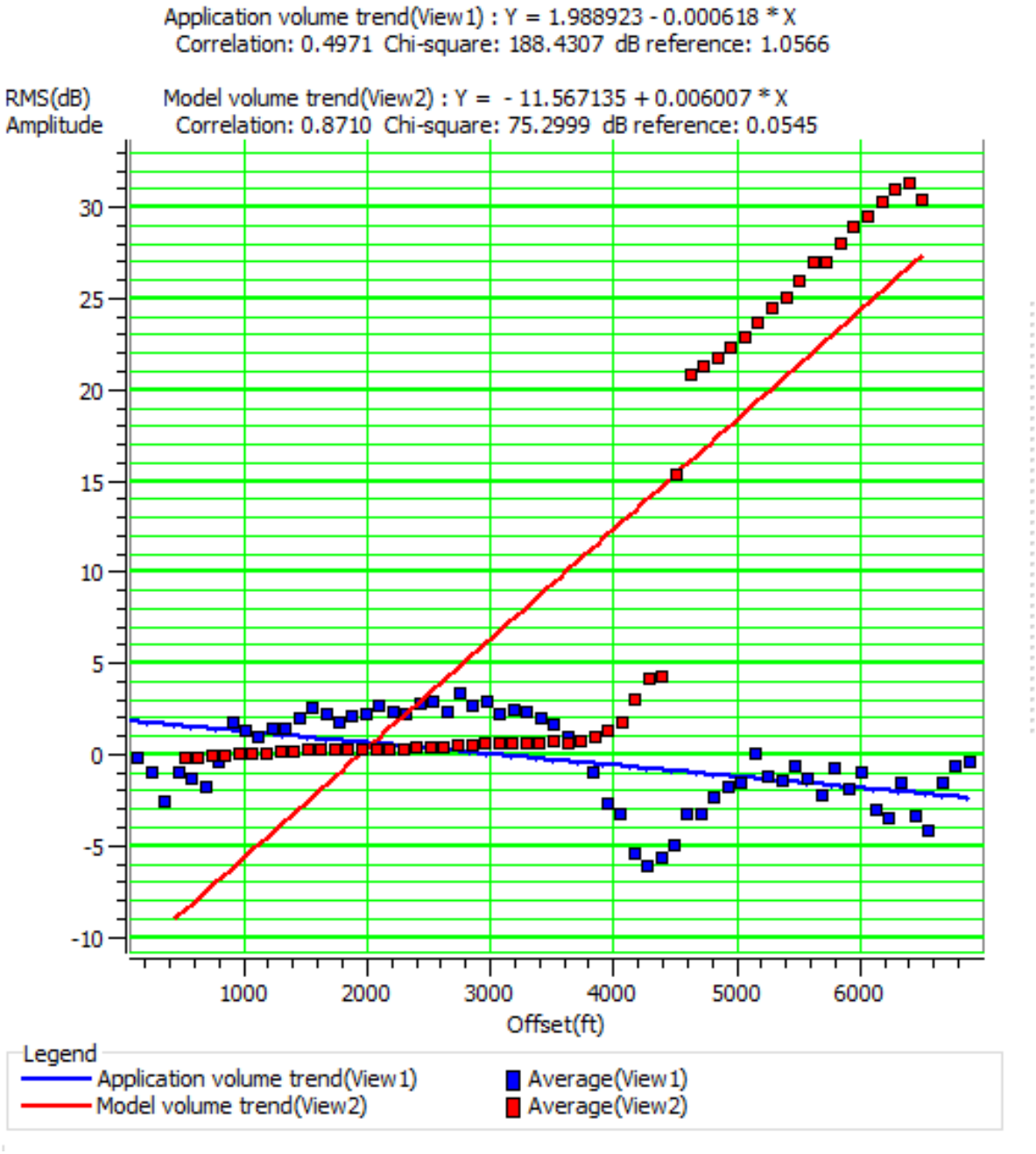

Figure C-1. The mean trend for the actual seismic gathers (blue) versus the mean gradient trend for the modeled volume (red). As you can see, they do not match each other. Generated in Hampson-Russell Software.

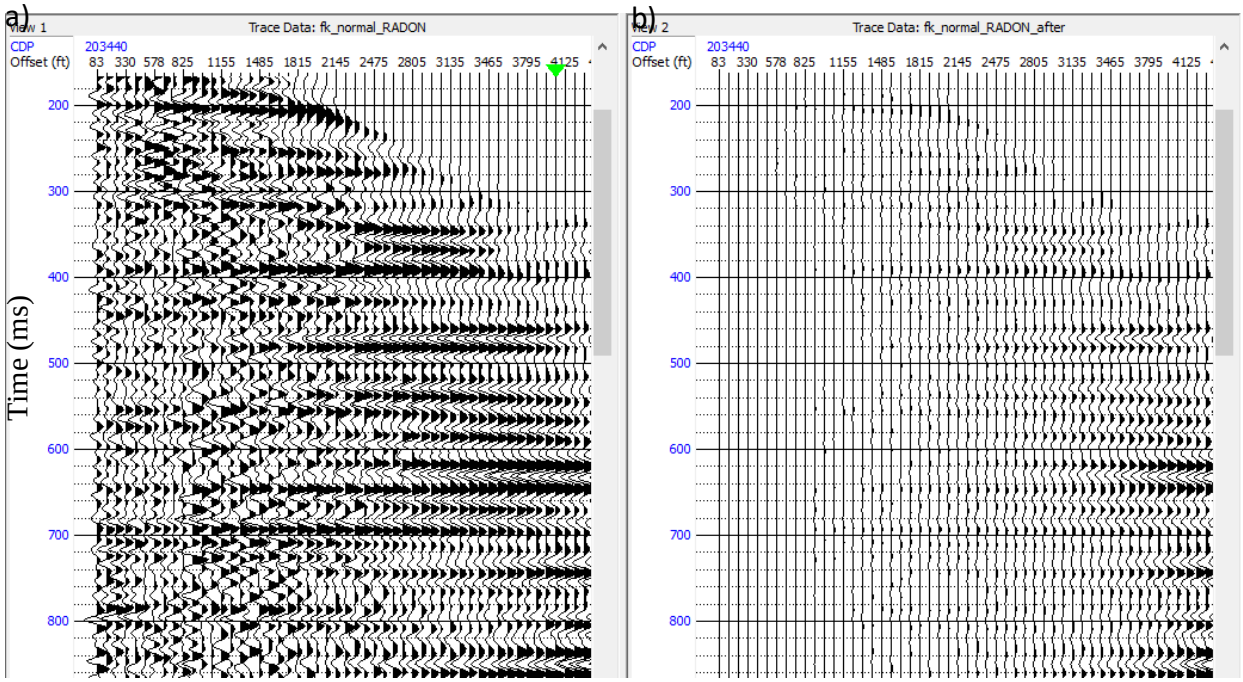

Figure C-2. a) The seismic data before AVO Offset Scaling. b) The seismic data after AVO Offset Scaling is applied. Time (ms) is on the y-axis with the Mississippian reservoir beginning around 640 milliseconds. Generated in Hampson-Russell Software.

REFERENCES

Adam, L., Batzle, M., and Brevik, I. (2006). Gassmann fluid substitution and shear modulus variability in carbonates at laboratory seismic and ultrasonic frequencies. *Geophysics, 71*(6), pp. F173-F183.

Altundas, Y. B., Chugunov, N., and Ramakrishnan, T. S. (2013). On the importance of accurate CO_2 fluid and fluid substitution models for the seismic monitoring of CO_2. *Society of Exploration Geophysicists 83rd Annual Meeting, Technical Program Expanded Abstracts Volume,* pp. 2716-2721.

Arts, R., Eiken, O., Chadwick, A., Zweigel, P. van der Meer, L., and Zinszner, B. (2004). Monitoring of CO_2 injected at Sleipner using time-lapse seismic data. *Energy, 29,* pp. 1383-1392.

Avseth, P., Mukerji, T., and Mavko, G. (2005). *Quantitative seismic interpretation: Applying rock physics to reduce interpretation risk*. New York, NY: Cambridge University Press.

Brown, S., Bussod, G., and Hagin, P. (2007). AVO monitoring of CO_2 sequestration: A benchtop-modeling study. *The Leading Edge, 26*(12), pp. 1576-1583.

Castagna, J. P., and Swan, H. W. (1997). Principles of AVO crossplotting. *The Leading Edge, 16*(4), pp. 337-344.

Castagna, J. P., Swan, H. W., and Foster, D. J. (1998). Framework for AVO gradient and intercept interpretation. *Geophysics, 63*(3), pp. 948-956.

Chadwick, R. A., Arts, R., Eiken, O., Kirby, G. A., Lindeberg, E., and Zweigel, P. (2004). 4-D seismic imaging of an injected CO_2 plume at the Sleipner field, central North Sea. *Geological Society of London, Memoirs, 29,* pp. 311-320.

Chadwick, A., Williams, G., Delepine, N., Clochard, V., Labat, K., Sturton, S., Buddensiek, M. L., Dillen, M., Nickel, M., Louise, A., Arts, R., Neele, F., and Rossi, G. (2010). Quantitative analysis of time-lapse seismic monitoring data at the Sleipner CO_2 storage operation. *The Leading Edge, 29*(2), pp. 170-177.

Chopra, S., and Castagna, J. P. (2014). Seismic Wave Propagation. In *AVO* (pp. 1-13). Tulsa, OK: Society of Exploration Geophysicists.

Colleary, W. M., Dolly, E. D., Longman, M. W., and Mullarkey, J. C. (1997). Hydrocarbon production from low resistivity chert and carbonate reservoirs in the Mississippian of Kansas. *American Association of Petroleum Geologists Rocky Mountain Section Meeting, Program Book and Expanded Abstracts Volume,* pp. 47-51.

Fadolalkarem, Y. (2015). Pre-stack seismic attribute analysis of the Mississippian chert and Arbuckle Group at the Wellington field, south-central Kansas. *Master's Thesis, University of Kansas*, pp. 1-118.

Graham, B., Tsoflias, G. P., and Watney, W. L. (2016). Seismic modeling of CO_2 fluid substitution in the Mississippian cherty dolomite and Arbuckle Group dolomite reservoirs, Wellington field, south-central Kansas. *Kansas Interdisciplinary Carbonate Consortium Annual Review Meeting, Abstracts Volume*, pp. 1-4.

Holubnyak, Y., Watney, L., Hollenbach, J., Birdie, T., FazelAlavi, M., Bidgoli, T., Schwab, D., Nolte, A., Tsoflias, G., Victorine, J., Graham, B., Doveton, J., Bruns, J., Blazer, B., and Wreath, D. (2017). Small scale field test demonstrating CO_2 sequestration in Arbuckle saline aquifer and by CO_2-EOR at Wellington field, Sumner County, Kansas. *Quarterly Progress Report to DOE-NETL*, pp. 1-10.

Ivanova, A., Bergmann, J. K., Yang, C., Lüth, S., and Juhlin, C. (2013). Seismic modeling of the AVO/AVA response to CO_2 injection at the Ketzin site, Germany. *Energy Procedia, 40*, pp. 490-498.

Kansas Geological Survey. (2018). Retrieved from http://www.kgs.ku.edu

Kansas Geological Survey. (2016, December 2). Data release notes, pp. 1-4.

Li, S., and Worsick, D. (2012, January 5). *AVO offset scaling in HRS-9*. Retrieved from https://www.cgg.com/technicalDocuments/cggv_0000015383.pdf

Lumley, D. E. (2001) Time-lapse seismic reservoir monitoring. *Geophysics*, *66*(1), pp. 50-53.

Montgomery, S. L., Mullarkey, J. C., Longman, M. W., Colleary, W. M., and Rogers, J. P. (1998). Mississippian "chat" reservoirs, south Kansas: low-resistivity pay in a complex chert reservoir. *American Association of Petroleum Geologists Bulletin, 82*(2), pp. 187-205.

Nissen, S. E., Carr, T. R. Marfurt, K. J., and Sullivan, E. C. (2009). Using 3-D seismic volumetric curvature attributes to identify fracture trends in a depleted Mississippian carbonate reservoir: Implications for assessing candidates for CO_2 sequestration. *American Association of Petroleum Geologists Studies in Geology, 59*, pp. 297-319.

Ratcliffe, A., and Roberts, G. (2003). Robust, automatic, continuous velocity analysis. *Society of Exploration Geophysicists 73rd Annual Meeting*, pp. 2080-2083.

Rutherford, S. R., and Williams, R. H. (1989). Amplitude-versus-offset variations in gas sands. *Geophysics, 54*(6), pp. 680-688.

Sirazhiev, A. (2012). Seismic attribute analysis of the Mississippian chert at the Wellington field, south-central Kansas. *Master's Thesis, University of Kansas*, pp. 1-129.

Smith, T. M., Sondergeld, C. H., and Rai, C. S. (2003) Gassmann fluid substitutions: A tutorial. *Geophysics, 68*(2), pp. 430-440.

Vega, S., Berteussen, K., Sun, Y. F., and Sultan, A. A. (2007). Is Gassmann the best model for fluid substitution in heterogeneous carbonates? *Society of Exploration Geophysicists 77th Annual Meeting, Expanded Abstracts*, pp. 1575-1578.

Watney, W. L., Guy, W. J., and Byrnes, A. P. (2001). Characterization of the Mississippian chat in south-central Kansas. *American Association of Petroleum Geologists Bulletin, 85,* pp. 85-113.

Watney, W. L., Rush, J., Wreath, D., Scheffer, A., FazelAlavi, M., Doveton, J., Barker, R., Newell, K. D., Datta, S., Roberts, J., and Fowle, D. (2013). Paleozoic anchor core in south-central Kansas – Berexco Wellington KGS #1-32. *American Association of Petroleum Geologists Mid-Continent Section Meeting, Mid-Continent Core Workshop: from Source to Reservoir to Seal*.

Yilmaz, O. (1987). Noise and multiple attenuation. In S. M. Doherty (Ed.), *Seismic data analysis: Processing, inversion, and interpretation of seismic data, Volume 1* (pp. 898-920). Tulsa, OK: Society of Exploration Geophysicists.